University of Tennessee, Knoxville
Trace: Tennessee Research and Creative Exchange

Masters Theses   Graduate School

5-2014

Microgrid Modeling and Grid Interconnection Studies

Hira Amna Saleem
University of Tennessee - Knoxville, hsaleem1@utk.edu

Recommended Citation

To the Graduate Council:

I am submitting herewith a thesis written by Hira Amna Saleem entitled "Microgrid Modeling and Grid Interconnection Studies." I have examined the final electronic copy of this thesis for form and content and recommend that it be accepted in partial fulfillment of the requirements for the degree of Master of Science, with a major in Electrical Engineering.

Kai Sun, Major Professor

We have read this thesis and recommend its acceptance:

Fred Wang, Fran Li

Accepted for the Council:
Dixie L. Thompson

Vice Provost and Dean of the Graduate School

(Original signatures are on file with official student records.)

Microgrid Modeling and Grid Interconnection Studies

A Thesis Presented for the
Master of Science
Degree
The University of Tennessee, Knoxville

Hira Amna Saleem
May 2014

ACKNOWLEDGEMENTS

DEDICATION

To my husband,
Ahmad

To my mother,
Sabiha

ABSTRACT

The demand for renewable energies and their integration to the grid has become more pressing than ever before due to the various reasons including increasing population energy demand, depleting fossil fuels, increasing atmospheric population, etc. Thus the vision of a sustainable future requires easy and reliable integration of renewable distributed generators to the grid. This master's thesis studies the dynamics of distributed generators when they are connected with the main grid. Simulink MATLAB is used for the design and simulations of this system. Three distributed generators are used in this system: Photo-voltaic converter, Fuel cell and diesel generator. The control and design of the power electronics converters is done to function properly in both grid-connected and islanding mode. The turbine governors in diesel generators control the proper functioning of diesel generator in both modes. The converters in both battery and PV make sure that they work properly in both grid-connected and islanding mode. The control of battery converter is designed in a way to function for load-shaving during unplanned load changes in the microgrid. This fully functioning microgrid is then connected with the main grid using Kundur's two-area system and simulated for various faults and load changes. A collection of data at the point of common coupling which is the point of connection of microgrid and main grid is gathered for various cases in the grid-connected mode. The cases for faults in the external grid are simulated and then WEKA software is used to develop decision trees. The development of the decision trees can help in predicting the decision of islanding of microgrid. By increasing this database for more scenarios; the response of the generators in grid and distributed generators in microgrid can be studied with decision trees giving more accurate results.

TABLE OF CONTENTS

LIST OF TABLES

LIST OF FIGURES

CHAPTER 1 : INTRODUCTION

Distributed Generation

The worldwide increase in demand of energy necessitates the use of different electric energy sources combined by a common grid for making an efficient electrical energy network. The distributed generation is becoming more and more popular compared to the conventional centralized system. In [1], the world scenarios are discussed as how the increasing demand of energy can be compensated. WADE is a non-profit organization which surveyed and then analyzed the energy profile of different countries and consequently, stressed the need of the full utilization of Distributed Electricity generation in order to keep up with the worldwide growing demand of energy. The share of decentralized power generation in the world market has increased to 7.2% by 2004, up from 7% in 2002. The long discussed and expected transition from a central power model to a 'hybrid' DE-central mix may possibly be underway, though slowly. WADE is optimistic that this market share will continue to expand [1].

The generation of highly reliable, good quality electrical power near the place where it is demanded can imply a change of paradigm. This concept, named distributed generation (DG), is especially promising when dispersed energy storage systems (fuel cells, compressed-air devices, or flywheels) and renewable energy resources (photovoltaic arrays, variable speed wind turbines, or combined cycle plants) are available. These resources can be connected through power conditioning ac units to local to local electric power networks also known as microgrids [2]. The distributed sources connection done with the grid should be in compliance with the IEEE 1547 standards. The penetration of distributed energy sources in the main grid is increasing and with it the need for the development of better and more reliable protection schemes is also increasing.

The few main advantages of distributed generation are given below:

1. The transmission and distribution cost is lowered.
2. Distributed Generation promotes the use of alternative energy sources and reliance on fossil fuels and nuclear power is reduced.
3. There is higher fuel efficiency because localized generation allows use of heat as well as generating electricity.
4. Distributed Energy Sources require less backup (as outage of a single generator cannot impact a system of many small generators), unlike a central system consisting of many large power plants. So, there are lesser chances of total black-out.

Microgrid

The DOE definition of microgrid is given below:

"A group of interconnected loads and distributed energy resources (DER) with clearly defined electrical boundaries that acts as a single controllable entity with respect to the grid (and can) connect and disconnect from the grid to enable it to operate in both grid-connected or island mode."

The heart of the microgrid concept is the notion of a flexible, yet controllable electronic interface between the microgrid and the familiar wider power system, or macro-grid. This interface essentially isolates the two sides electrically; and yet connects them economically by allowing delivery and receipt of electrical energy and ancillary services at the interface [5].The consideration of bidirectional power flow between microgrid and main grid puts forward many challenges in terms of protection and reliability.

Types of fault

Most faults in an electrical utility system with a network of overhead lines are one-phase-to-ground faults resulting primarily from lightning-induced transient high voltage and from falling trees and tree limbs. Momentary tree contact caused by wind, ice, freezing snow, and wind during severe storms are other causes of fault. These faults include the following, with very approximate percentages of occurrence [3]:

<div align="center">

Single phase-to-ground: 70%–80%
Phase-to-phase-to ground: 17%–10%
Phase-to-phase: 10%–8%
Three-phase: 3%–2%

</div>

In conventional network, power flows from higher voltage level to lower voltage level and in case of fault short circuit current decrease as distance increase. Modern Microgrid has been changed the concept and power could flow in both direction. Some of the prominent protection issues are: short circuit power, fault current level and direction, device discrimination, reduction in reach of over-current relays, nuisance tripping, protection blinding, etc [4].

Modeling of Microgrid

Simulink MATLAB is used to model microgrid in this project. Three distributed generators (Lead-acid battery, diesel generator and PV) are used in this microgrid. The location of the distributed generators is chosen to be close to each other so that they can support each other in functioning.

IEEE 13 Node Test Feeder System

A benchmarked radial distribution was used to develop the load and lines model of microgrid model to help in comparative studies. IEEE 13 Node test feeder system shown in Figure 1.1 was used for this purpose. Some of the characteristics of this system are given below:

1. It is small but heavily loaded at 4.16kV.
2. It has unbalanced spot and distributed loads.
3. It consists of lines with unbalanced phasing.
4. Shunt capacitor banks.

Bus 650 is the interconnection point of microgrid and main grid and is called "Point of Common Coupling (PCC)". Power can flow in both directions at this point.
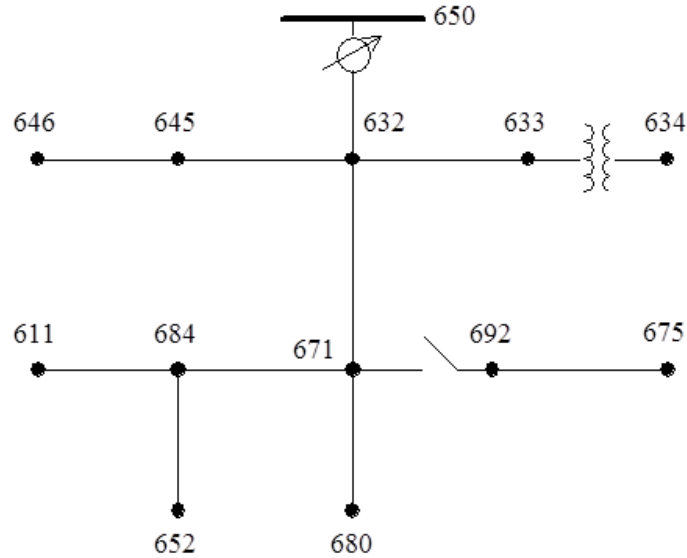
Figure 1.1. Network topology of IEEE 13 Node Test Feeder System.

The details of this IEEE 13 Node test feeder model as specified by IEEE in [6] are given below:

Table 1.1 Overhead Line Configuration Data.

Config.	Phasing	Phase	Neutral	Spacing
		ACSR	ACSR	ID
601	B A C N	556,500 26/7	4/0 6/1	500
602	C A B N	4/0 6/1	4/0 6/1	500
603	C B N	1/0	1/0	505
604	A C N	1/0	1/0	505
605	C N	1/0	1/0	510

Table 1.2 Underground Line Configuration Data.

Config.	Phasing	Cable	Neutral	Space ID
606	A B C N	250,000 AA, CN	None	515
607	A N	1/0 AA, TS	1/0 Cu	520

Table 1.3 Line Segment Data.

Node A	Node B	Length(ft.)	Config.
632	645	500	603
632	633	500	602
633	634	0	XFM-1
645	646	300	603
650	632	2000	601
684	652	800	607
632	671	2000	601
671	684	300	604
671	680	1000	601
671	692	0	Switch
684	611	300	605
692	675	500	606

Table 1.4. Transformer Data.

	kVA	kV-high	kV-low	R - %	X - %
Substation:	5,000	115 - D	4.16 Gr. Y	1	8
XFM -1	500	4.16 – Gr.W	0.48 – Gr.W	1.1	2

Table 1.5. Capacitor Data

Node	Ph-A	Ph-B	Ph-C
	kVAr	kVAr	kVAr
675	200	200	200
611			100
Total	200	200	300

Table 1.6. Regulator Data.

Regulator ID:	1		
Line Segment:	650 - 632		
Location:	50		
Phases:	A - B -C		
Connection:	3-Ph,LG		
Monitoring Phase:	A-B-C		
Bandwidth:	2.0 volts		
PT Ratio:	20		
Primary CT Rating:	700		
Compensator Settings:	Ph-A	Ph-B	Ph-C
R - Setting:	3	3	3
X - Setting:	9	9	9
Volltage Level:	122	122	122

Table 1.7. Spot Load Data.

Node	Load	Ph-1	Ph-1	Ph-2	Ph-2	Ph-3	Ph-3
	Model	kW	kVAr	kW	kVAr	kW	kVAr
634	Y-PQ	160	110	120	90	120	90
645	Y-PQ	0	0	170	125	0	0
646	D-Z	0	0	230	132	0	0
652	Y-Z	128	86	0	0	0	0
671	D-PQ	385	220	385	220	385	220
675	Y-PQ	485	190	68	60	290	212
692	D-I	0	0	0	0	170	151
611	Y-I	0	0	0	0	170	80
	TOTAL	1158	606	973	627	1135	753

Table 1.8. Distributed Load Data.

Node A	Node B	Load	Ph-1	Ph-1	Ph-2	Ph-2	Ph-3	Ph-3
		Model	kW	kVAr	kW	kVAr	kW	kVAr
632	671	Y-PQ	17	10	66	38	117	68

The total load at all three phases in the microgrid is unbalanced and is given below:
Active Power:
> A-phase: 1.175 MW
> B-phase: 1.039 MW
> C-phase: 1.625 MW

Reactive Power:
> A-phase: 416 kVAR
> B-phase: 465kVAR
> C-phase: 878kVAR

The IEEE 13 Node Test Feeder Model developed in MATLAB Simulink is shown in Figure 1.2.
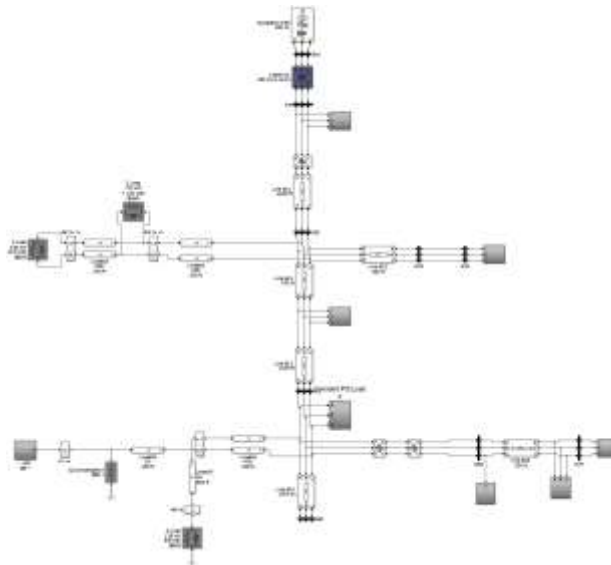
Figure 1.2. Simulink Model of IEEE 13 Node Test Feeder System.

CHAPTER 2 : DIESEL GENERATOR

A diesel generator consists of a diesel engine with an electric generator to generate electrical energy. A diesel generator is chosen to be installed in the microgrid installed; it will be of much higher power capacity than battery and PV and will support the grid.

Emergency standby diesel generators, for example such as those used in hospitals, water plant, are, as a secondary function, widely used in the US and the UK (Short Term Operating Reserve) to support the respective national grids at times for a variety of reasons. In the UK for example, some 0.5 GW of diesels are routinely used to support the National Grid, whose peak load is about 60 GW. These are sets in the size range 200 kW to 2 MW. This usually occurs during, for example, the sudden loss of a large conventional 660 MW plant, or a sudden unexpected rise in power demand eroding the normal spinning reserve available [7].

Design and Modeling

A three-phase generator rated 3.125 MVA, 2.4kV is connected to a 4.16 kV network through a Delta-Y 5 MVA transformer.

Hydraulic Turbine Governor (Grid-mode)

In grid connected mode, operational control of voltage and frequency is done entirely by the grid; however, microgrid still supplies the critical loads at PCC, thus acts as a PQ bus. The electricity from the main grid is used as a reference and the hydraulic turbine governor of generator maintains and follows this frequency. The Hydraulic Turbine and Governor block in Simulink uses a nonlinear hydraulic turbine model, a PID governor system, and a servomotor as shown in Fig.2.1.
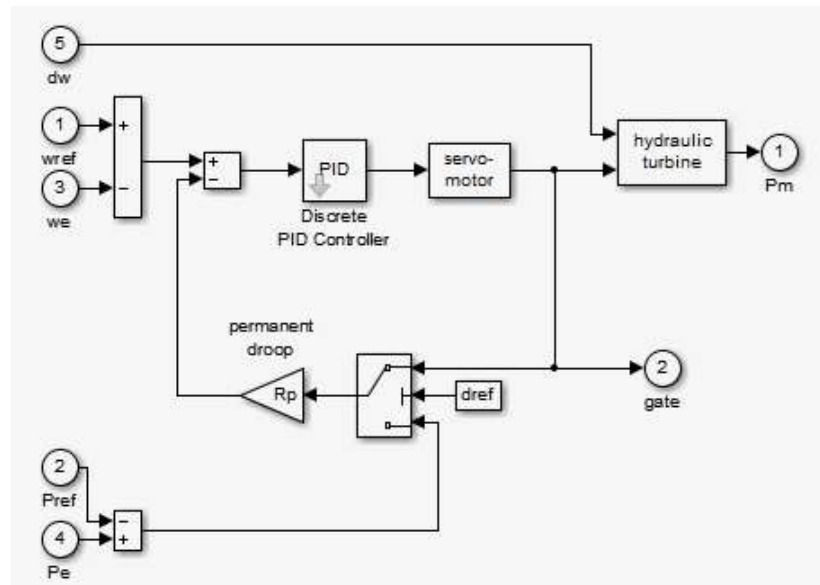
Figure 2.1. Hydraulic Turbine Governor model in Simulink MATLA

6

Diesel Engine Governor (Islanding-mode)

In islanding mode, there is no reference signal from the main grid. In this microgrid model, generator provides the reference signal in the microgrid and controls the voltage and frequency using the diesel engine governor. The Simulink model of the Diesel engine governor implements the actuator control as shown in Fig.2.2.
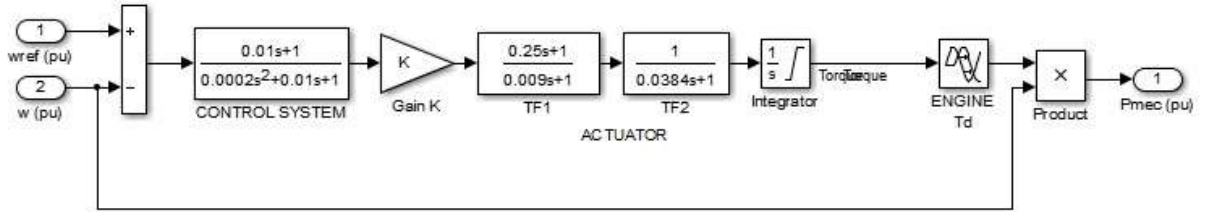
Figure 2.2. Simulink block of Diesel Engine Governor

Transformer:

A step-up transformer of 5 MVA is used to step up the voltage from the diesel generator to the voltage level of 4.16kV in the microgrid. The transformer steps up voltage from 2.4 kV to 4.16kV.

Simulink Model

The Simulink model used is show below in Fig.2.3.
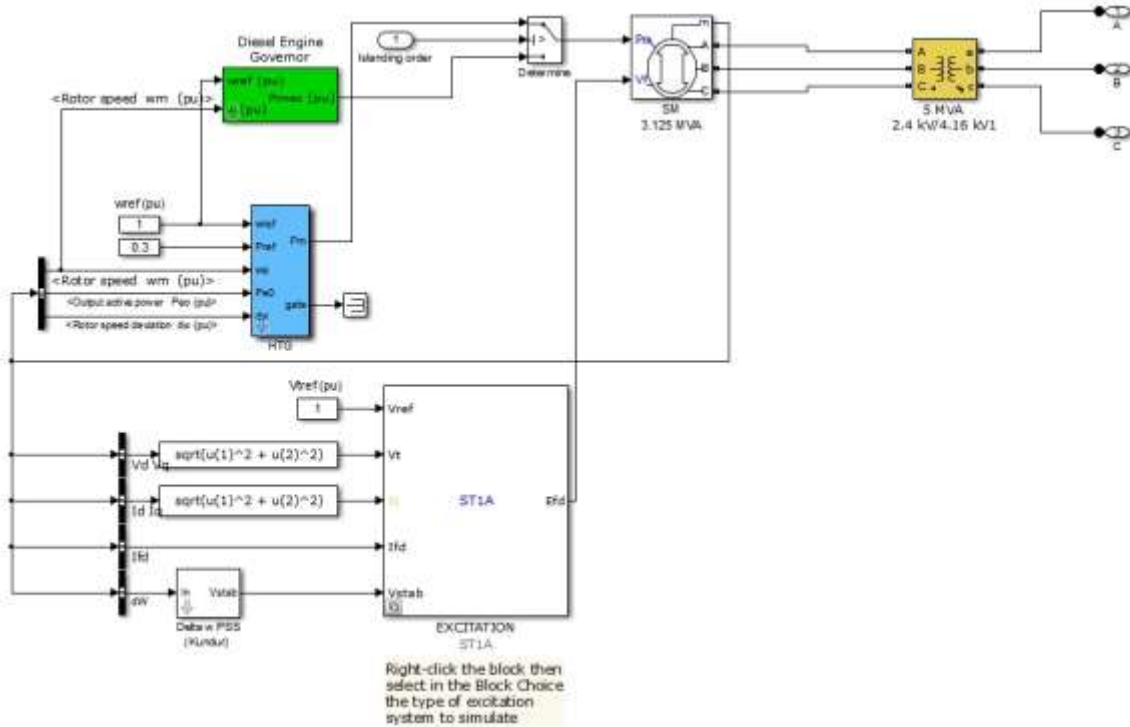
Figure 2.3. Simulink model of Diesel Generator.

7

CHAPTER 3 : PHOTOVOLTAIC ENERGY SOURCE

The source of photovoltaic energy is sun which is 150 million kilometer away from Earth. It is such a big source of energy that in one minute, the Earth receives enough energy from the Sun to meet our needs for a year. It is also easily accessible and free of cost. The solar energy can be used directly for heating, lighting, cooking, drying and for generating electricity. On a large scale, this solar energy can be utilized for commercial and industrials use aswell. Winds and waves are also consequences of the solar energy. The thermal energy from sun is converted to electricity using solar cells. The direct current (DC) electricity created in this way is then converted to alternating current (AC) or stored for later use.

Importance of PV in energy production

Photovoltaics is a fast growing market and holds a promising future. Worldwide in 2011 about half of the previously cumulated PV module capacity entered the market. Now PV technology is being increasingly recognized as a part of the solution to the growing energy challenge and an essential component of future global energy production. PV system performance has strongly improved. The typical Performance Ratio has increased from 70 % to about 85 % over the last 15 years. Germany including other European country contributed to major role towards the global cumulative PV installation until 2011, that is, 70% of global PV installation [8].

Design and Modeling

PV model of 0.6 MW capacity is designed in Simulink MATLAB. Average models of converter are used to emulate the converter behavior which is controlled by PQ-Control strategy and then the output is stepped up to the network voltage level of 4.16kV.

Maximum Power Point Tracking (MPPT):
Irradiance data from solar radiation is input to output the DC voltage based on the Maximum Power Point Tracking (MPPT).

Power output of a Solar PV module changes with change in the direction of sun, changes in solar irradiance level and variations in temperatures. It is known that the efficiency of the solar PV module is low and it is in the range of 13%. Since, the module efficiency is low it is desirable to operate the module at the peak power point so that the maximum power can be delivered to the load under varying temperature and irradiance conditions. Hence maximization of power, improves the utilization of the solar PV module. A maximum power point tracker (MPPT) is used for extracting the maximum power from the solar PV module and transferring that power to the load. Considering the investment cost of the PV system, it is always a prerequisite to operate PV at its Maximum Power Point (MPP) [9].

Average model of DC-DC converter and three-phase inverter:

After the conversion of solar energy to DC, an average model of DC-DC converter is used to step up the voltage. This stepped up DC voltage is then converted to alternating current (AC) by an average model of three-phase inverter.

An inductor of 6.74µH is used to reduce the current harmonics at the output of the PV converter.

Active and Reactive Power control of converter:

Current controlled based PQ Control Strategy is used to provide reference 'd' and 'q' components which are then input to the average model of converter. The reference reactive power in PV is a constant value in grid-connected mode but in islanding mode, a droop control is used to follow the reactive power in the islanded microgrid.

Transformer:

A step-up transformer of 0.5 MVA is used to step up the voltage of PV to the voltage level of 4.16kV in the microgrid. The transformer steps up voltage from 0.48kV to 4.16kV.

Simulink Model

The Simulink model used is show below in figure.
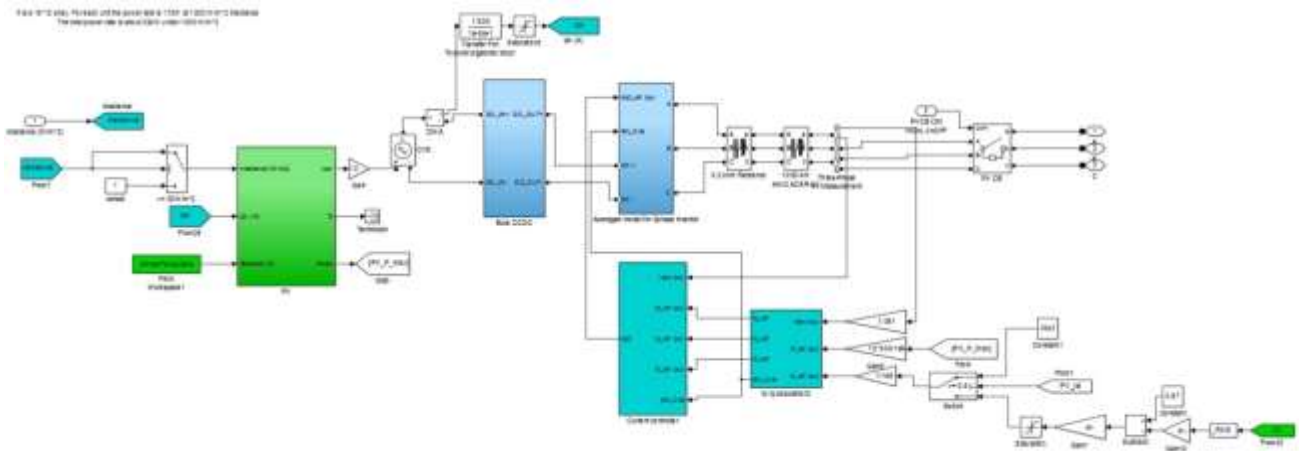
Figure 3.1. Simulink model of PV.

9

CHAPTER 4 : BATTERY

Fuel Cells are a popular distributed energy source. They can be used for hospitals, offices, residential areas or to supply power at remote places like construction areas. Lead-acid batteries have comparatively lower energy density but they are cheaper and hence, more suitable for large systems where weight is not a concern.

Lead-Acid Battery

Renewable energy systems like Solar and Wind are intermittent in nature. For stand-alone applications they often require energy storage systems to provide the fill in power. Batteries have been traditionally used to provide the fill-in power for solar and wind systems
The Lead Acid Battery is one of the widely used electrochemical energy storage systems. This can be attributed to its chemical and physical properties that makes it an ancient system and suitable for a variety of applications [22]. A few of these properties are given below [22].

- The reactants are solids of low solubility which causes a stable voltage and highly reversible reactions.
- Both electrodes contain only lead and lead compounds as active material that does not require conducting additives.
- It has a high cell voltage of 2V.
- Lead Acid technology is cheaper than most technologies and is the primary reason.

A lead acid battery is used to compensate the ups and downs in the grid-tied voltage during grid-connection mode. In islanding mode, the same battery is used to fulfill the load requirements. In [2], a 34 MW NAS Battery is used to stabilize the output of a 51 MW Wind Turbine farm in the Tahoku district of Japan. The fluctuations in the power supplied by the wind turbine are stabilized with a precision of +-2% using the battery.

Design and Modeling

The simulation of charge and discharge of a battery model using parameters taken from a steady state curve is done in [10]. The approximate error between simulation results and experimental results varies between 5% to 10% [10]. The battery model block in Simulink is used to get the simulation results in [10]. The battery block in Simulink implements set of predetermined charge behavior for four types of battery: Lead-Acid, Lithium-Ion, Nickel-Cadmium and Nickel-Metal-Hydride. The Lead-Acid Battery Model is therefore used to emulate the exact behavior of a real lead-acid battery. The lead-acid battery used with its parameters is shown in Fig.4.1
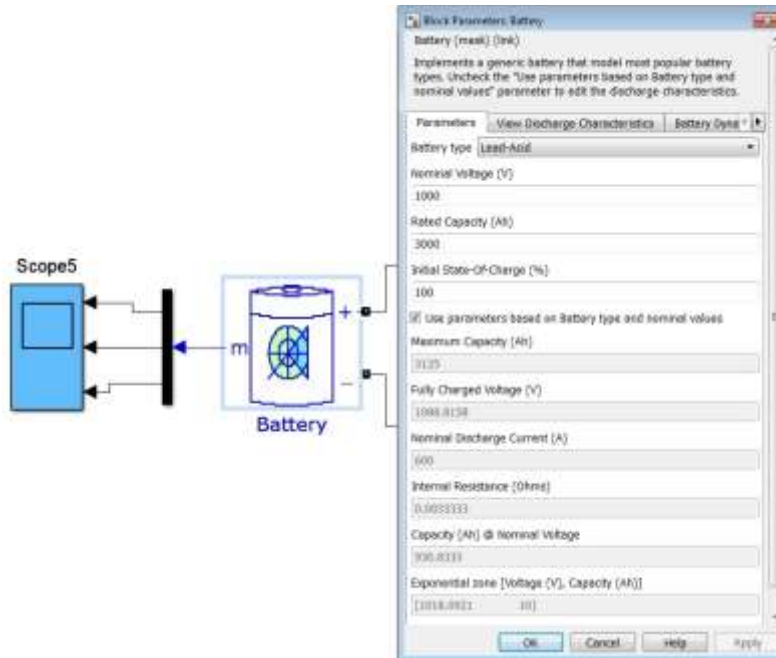
Figure 4.1. Simulink model of lead-acid battery with its parameters

Bi-directional Converter:

Bidirectional converter is used in electric vehicles for efficient utilization of battery by providing a uniform voltage supply and re-charging the battery at some instances e.g down-slope motion of car [12-14]. A bidirectional voltage source converter shown in Fig.4.2 is used in the battery converter design. This converter acts as a buck converter when the battery discharges and the current flows from battery to the main grid. Otherwise, it acts a boost converter when the battery charges and the current flows from the main grid to the battery.
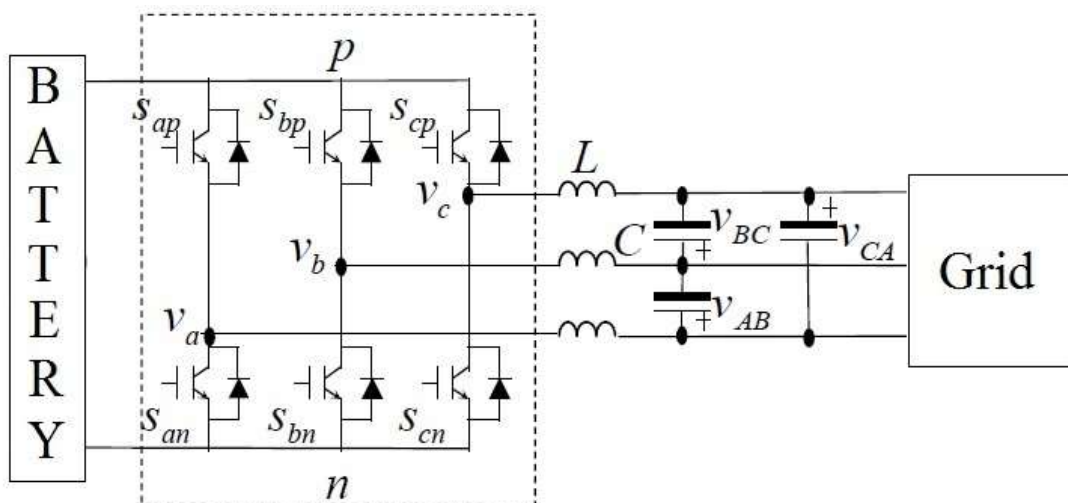
Figure 4.2. Bi-directional Voltage Source Converter

Real/reactive Power Controller:

The main purpose of this controller is to control the instantaneous real and reactive power that this battery exchanges with the microgrid side. The flow and direction of the current is controlled by controlling the PWM given to this converter. The total power for which the converter is designed is 0.15 MW and the lead-acid battery of 1088 V is selected. Switching frequency of 8kHz is used to generate the PWM for the converter; the PWM is generated using the dq- frame of reference. PQ control strategy is used for this purpose.
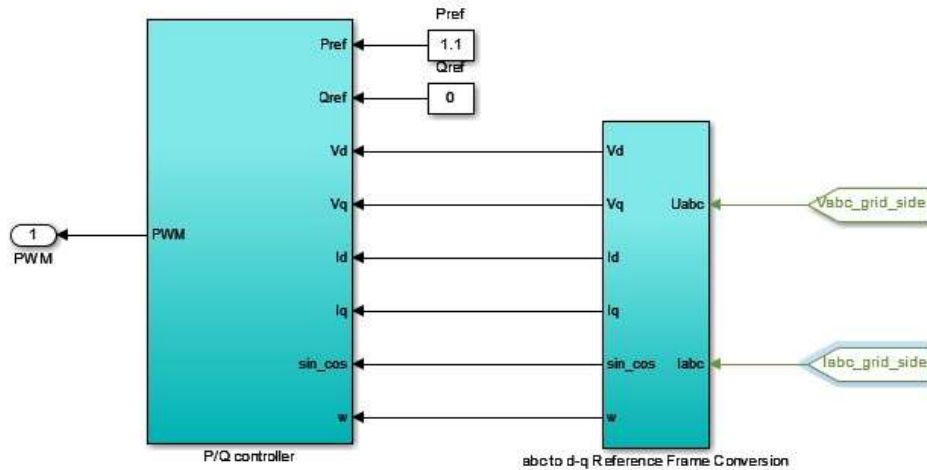
Figure 4.3. P-Q Controller for battery

In this microgrid connected VSC system, the real and reactive power output of the battery converter is proportional to the d- and q-axis components of the converter current, respectively. The angle of the grid-connected side is calculated using the phase-locked loop (PLL) of voltage at that point and provided to the controller.

LCL Filter:

Harmonic current is injected by the voltage source converter used which is controlled by PWM switching. Therefore, an AC filter is used on the grid side of the converter to filter the high frequency harmonics injected by the converter. An LCL filter as shown in Figure 4.4 is used to remove these harmonics.

3mH

120uF

26.41 uH
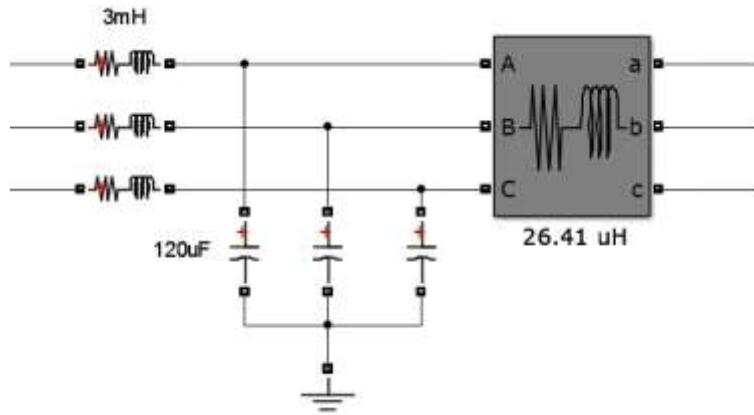
Figure 4.4. LCL filter for batter

Transformer:

A step-up transformer is used to step up the voltage of the battery to the voltage level of 4.16kV in the microgrid. The transformer steps up voltage from 220V to 4.16kV.

Simulink Model

The Simulink model used is show below in Figure 4.5.
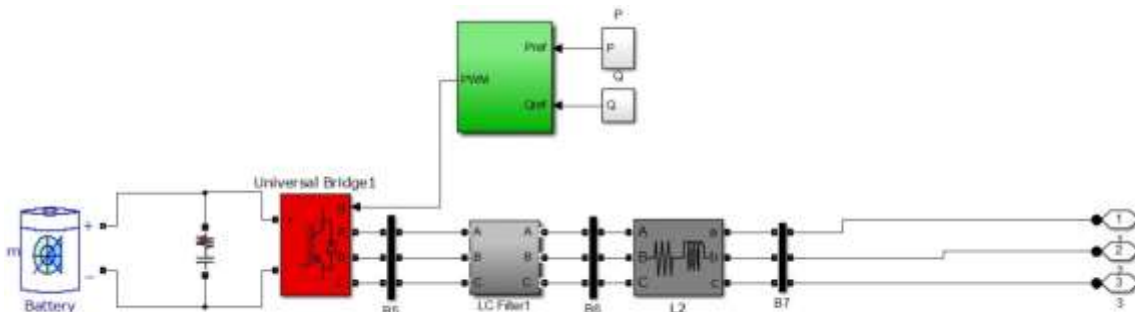
Figure 4.5. Simulink model of Battery

CHAPTER 5 : CONTROL STRATEGIES IN MICROGRID

The control of a microgrid to ensure a reliable and stable supply is very important for the safety and stability of main grid. The microgrid model made can work in both grid-connected and islanding mode. The operation in both the modes is controlled with the help of convertor controllers in each distributed generator. The control strategies used in both modes are explained below.

Islanding Mode

In islanding mode, there is no reference signal from the main grid. The microgrid operates independently and acts like a PV bus with hydraulic turbine governor controlling the frequency. In this microgrid model, generator provides the reference signal in the microgrid and controls the voltage and frequency using the diesel engine governor. The Simulink model of the Diesel engine governor implements the actuator control as shown in Fig.5.1.
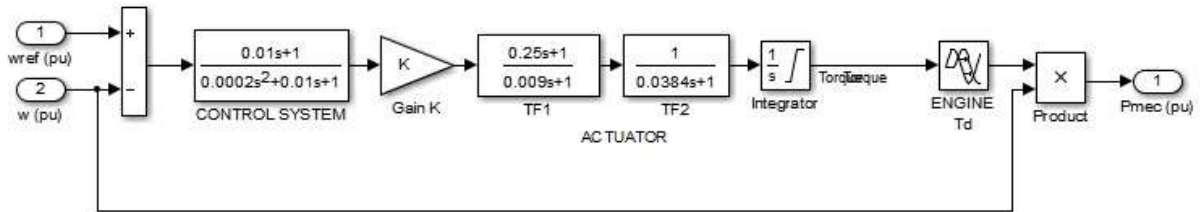
Figure 5.1. Simulink block of Diesel Engine Governor

Battery and PV operate in PQ mode; the PQ control design explained in [16] is used and is shown below.
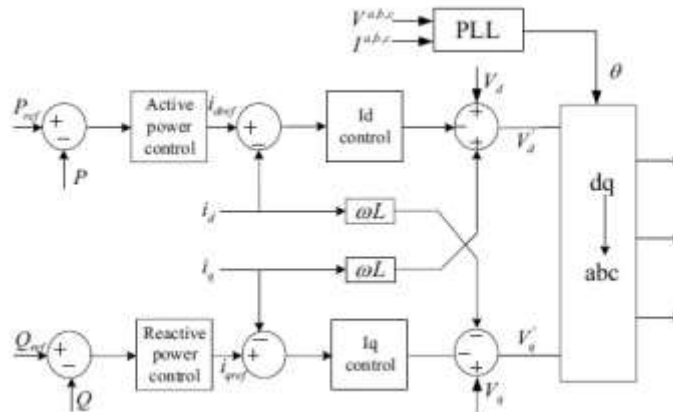
Figure 5.2. PQ- control design [16].

This PQ control consists of an inner current control loop and the control structure contains an inner and an outer voltage control loop. The control mechanism is performed in 'dq' reference frame rotating at the fundamental frequency. This fundamental frequency is calculated form the PLL using the voltage and current at the output of the converter for Park's Transformation. The benefit of using the 'dq' reference frame is that the sinusoidal command tracking problem is

14

converted to an equivalent DC command tracking problem. Therefore, PI compensators can be used in the control design. Also, by using integral in compensator an almost zero steady-state tracking error can be attained.

The reference reactive power in PV is a constant value in grid-connected mode but in islanding mode, a droop control is used to follow the reactive power in the islanded microgrid.

Grid-Connected Mode

In grid connected mode, operational control of voltage and frequency is done entirely by the grid; however, microgrid still supplies the critical loads at PCC, thus acts as a PQ bus. The electricity from the main grid is used as a reference and the hydraulic turbine governor of generator maintains and follows this frequency. The Hydraulic Turbine and Governor block in Simulink uses a nonlinear hydraulic turbine model, a PID governor system, and a servomotor as shown in Fig.5.3.
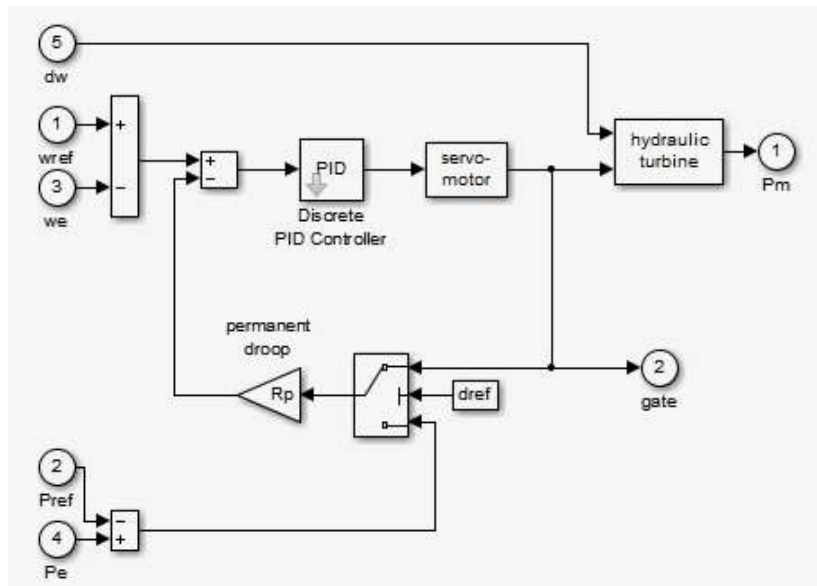
Figure 5.3. Hydraulic Turbine Governor model in Simulink MATLAB

Battery and PV operate in PQ mode ; the abc- reference frame in these controllers is converter to 'dq' reference frame. The signals in steady-state are turned to DC waveforms which can be controlled more easily using PI controllers. The PQ designed controller used by battery and PV is based on the Fig.5.2.

Battery control for Power-Shaving

The battery is used as a compensator to minimize the variation of the PCC MW flow relative to the planned amount. Fig.5.4 shows the flow of power throughout the microgrid.
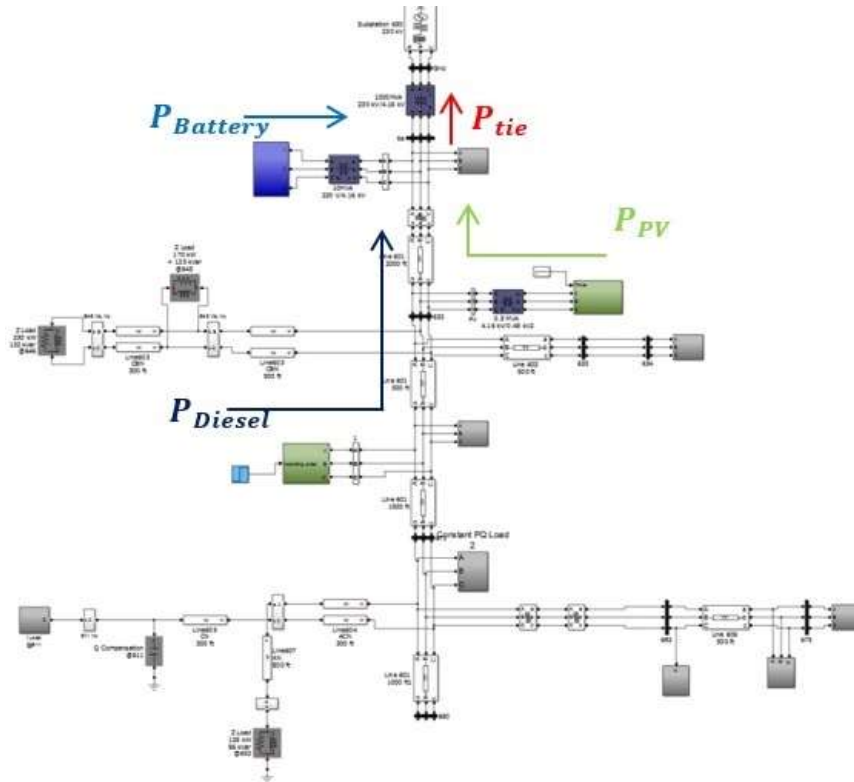
Figure 5.4. Microgrid Power flow diagram

Battery control is designed to shave power above and below a reference value for both grid-connected and islanding mode.

That is minimizing,

$$\Delta P_{tie} = P_{tie} - P_{tie\_planned} \qquad (5.1)$$

If $\Delta P_{tie} > 0$, battery is charged. Otherwise, battery is discharged. For this purpose, an additional control is added to the PQ controller design of battery as shown in Fig.5.5.
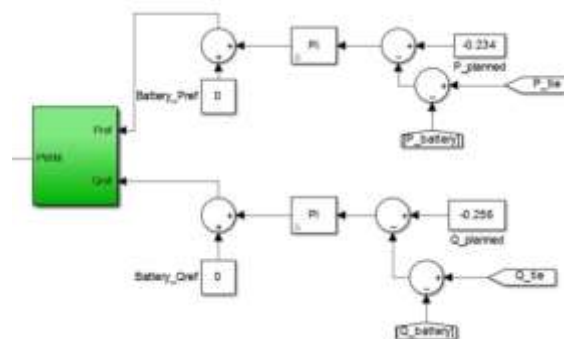
Figure 5.5. Battery charge and discharge control for power shaving.

The error which is the difference of the active and reactive power flow through the tie-line and the planned flow is passed through a compensator and then added to the desired battery power

16

which we want it to operate at and thus give the reference active and reactive power for the PQ-controller of battery. Also, the active and reactive power of battery is subtracted from that through tie-line so that the power produced by battery does not affect the output reference power of controller.

For 100kW load increase in microgrid,
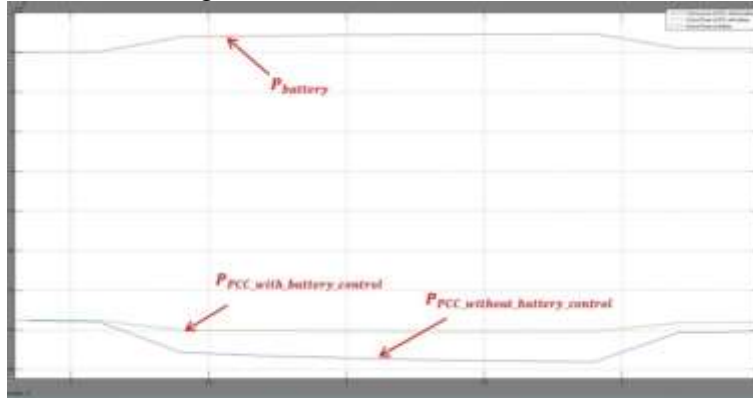
Figure 5.6. Power levelling by using battery to discharge for 100kW load increase of load in microgrid.

From the Fig.5.6, there is substantial levelling of the active power at PCC by using battery when there is an abnormal load shift in microgrid. In this way, the battery can be used to shave peak load change. Whenever the power flow through PCC changes from the planned value, battery will charge and discharge accordingly to minimize the impact of the unplanned load on the power flow at PCC.

IEEE 1547 Standard Adherence

The 1547 standard is the only systems-level technical standard of uniform requirements and specifications universally needed to interconnect distributed energy resources with the grid.

Current Harmonics:

According to IEEE 1547 Standard, when the DR is serving balanced linear loads, harmonic current injection at PCC shall not exceed the limits stated below [15].

Table 5.1. Current Harmonics Standard in IEEE 1547.

IEEE Std 1547.2-2008
IEEE Application Guide for IEEE Std 1547™, IEEE Standard for Interconnecting Distributed Resources with Electric Power Systems

Maximum harmonic current distortion in percent of current (I) [a]

Individual harmonic order (odd harmonics)[b]	$h < 11$	$11 \leq h < 17$	$17 \leq h < 23$	$23 \leq h < 35$	$35 \leq h$	Total demand distortion
Percent (%)	4.0	2.0	1.5	0.6	0.3	5.0

[a] I = The greater of the local EPS maximum load current integrated demand (15 min or 30 min) without the DR unit or the DR unit rated current capacity (transformed to the PCC when a transformer exists between the DR unit and the PCC).

[b] Even harmonics are limited to 25% of the odd harmonic limits shown.

17

The harmonics injected by the diesel generator satisfy the limitations stated in table 5.1 and are shown in the Fig.5.7 below:
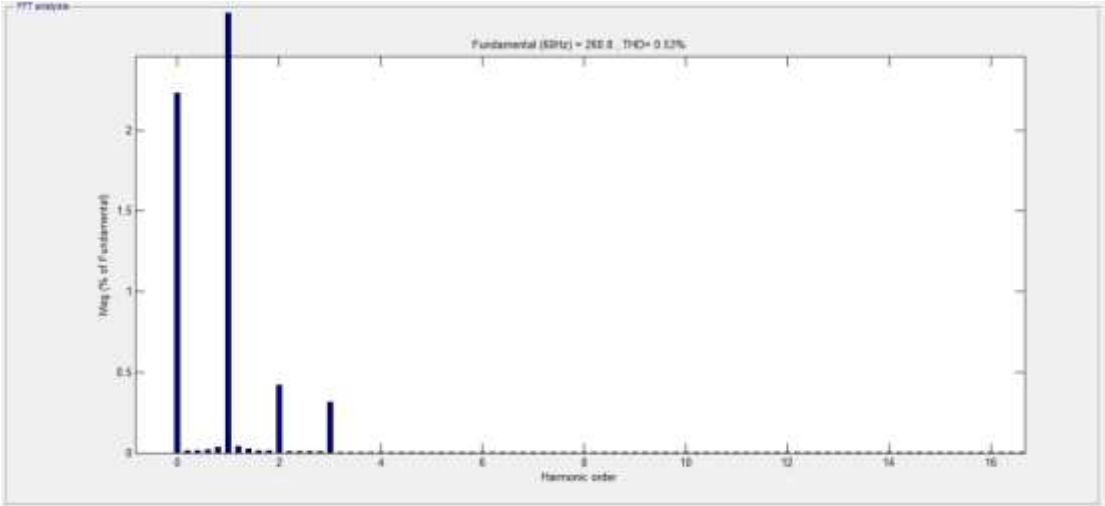
Figure 5.7. Current Harmonics injected by Diesel Generator.

The harmonics injected by PV converter satisfy the limitations stated in table 5.1 and are shown in the Fig.5.8 below:
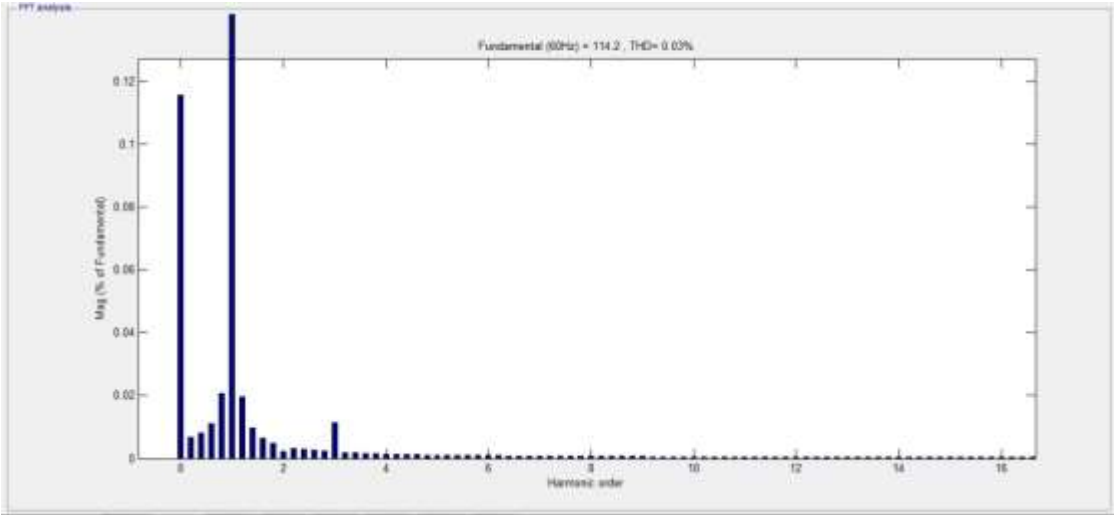
Figure 5.8. Current Harmonics injected by PV.

The harmonics injected by the battery converter satisfy the limitations stated in Table 5.1 and are shown in the figure below:
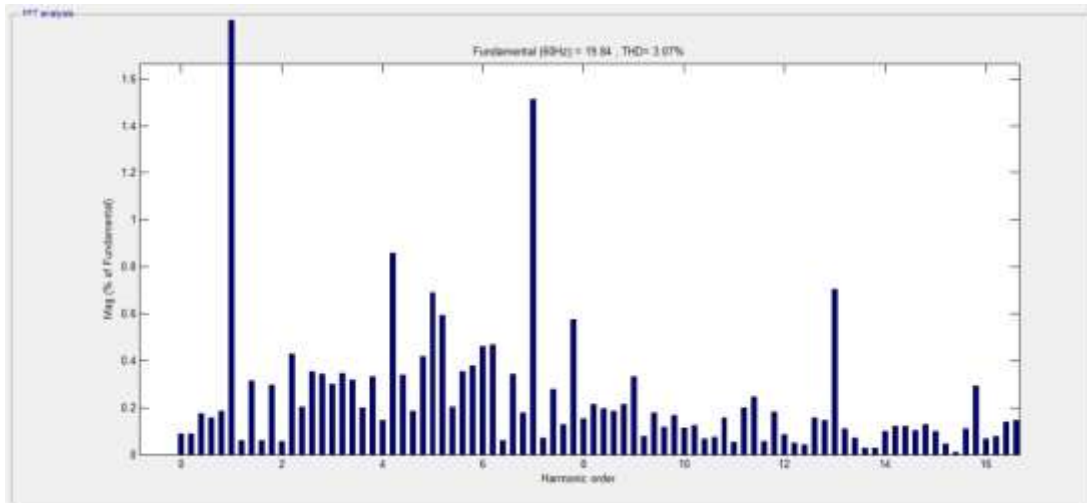
Figure 5.9. Current Harmonics injected by battery.

DC Injection:

According to the limitation of dc injection in IEEE Standard 1547-2003[15]:

> "The DR and its interconnection system shall not inject dc current greater than 0.5% of the full rated output current at the point of DR connection."

These limitations are satisfied by all three Distributed Generators as shown in the Table 5.2 below.

Table 5.2. DC Current Injected by DGs.

Distributed Generators	DC Injection Current (A)
Battery	0.0178
PV	0.137
Generator	5.8
Total DC Injection Current	5.95 <6.5 (0.5% of full rated output current)

CHAPTER 6 : SIMULATIONS AND RESULTS

Grid Interconnection

The motivation and benefits of connecting the distributed generators to main grid are given below:

1. Stable Operation:
    The power grid acts a 'stiff' source and facilitates stable operation of microgrid.
2. Availability:
    Grid is available easily to take care of load in microgrid in cases when the distributed generators in microgrid may go down.
3. Economics:
    The extra electricity generated by microgrid can be sent to grid and sold for economic benefits. Also, electricity from grid can be used at times like night when the output of PV is low and the price of electricity is cheaper at grid.

An ideal voltage source can be used as grid in Simulink. The three DGs are placed closer to each other so that they operate properly as shown in Figure 6.1.
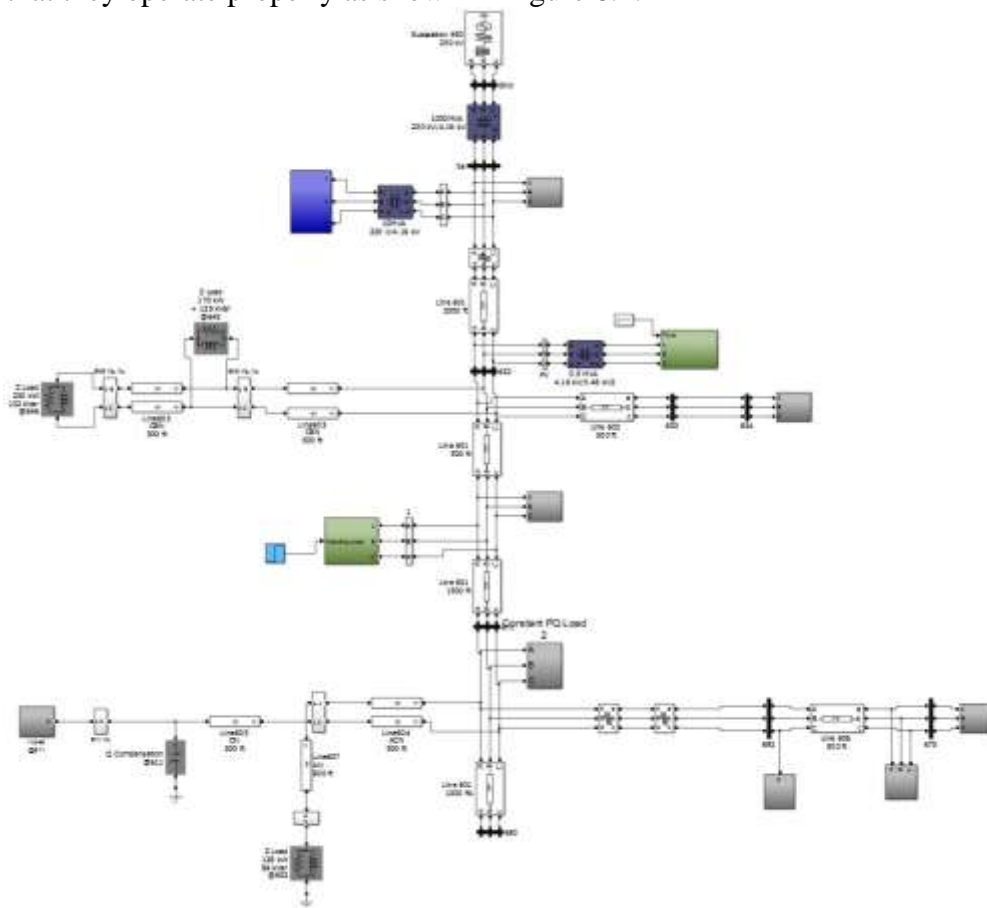
Figure 6.1. Simulink model of Microgrid.

The following three contingencies simulations are done in grid-mode in order to study and analyze the behavior of the microgrid.

1. IEEE 13 Feeder Microgrid with single-phase 4-cycles fault at PCC.
2. IEEE 13 Feeder Microgrid with three-phase 4-cycles fault at Bus 633 near PV and PV is turned off during fault.
3. IEEE 13 Feeder Microgrid with sudden load change.

1. *Single-phase 4-cycles fault at PCC*

The 4-cycles fault is introduced at PCC as shown in Figure 6.2.
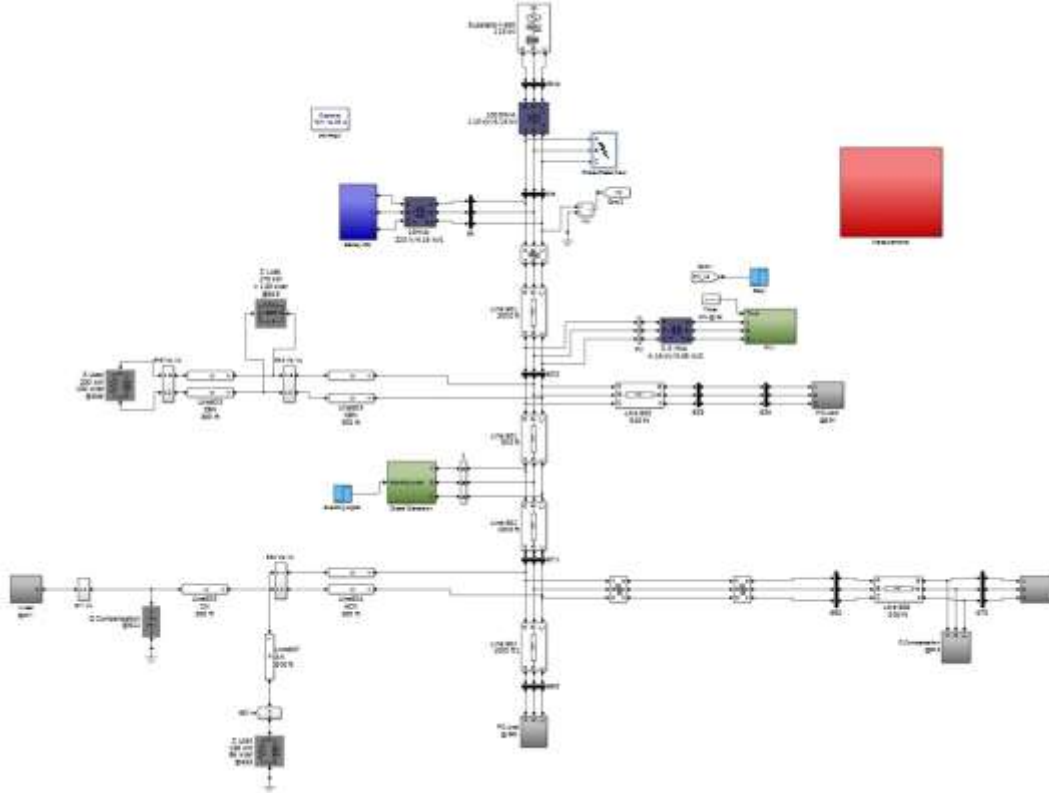
Figure 6.2. Single-phase 4-cycles fault at PCC in Simulink model of Microgrid.

The voltage, current, active power and reactive power simulation results at PCC are shown in Fig.6.3.The PCC voltage attains its steady state value in about 0.1 second after fault. There is a huge dip in the reactive power but the active power remains almost constant. Since it's a single phase fault, the variations in the voltage and current of all three phases are different during the duration of fault. The active and reactive power at PCC is flowing from the main grid to microgrid but during the duration of fault the flow of the reactive power reverses.
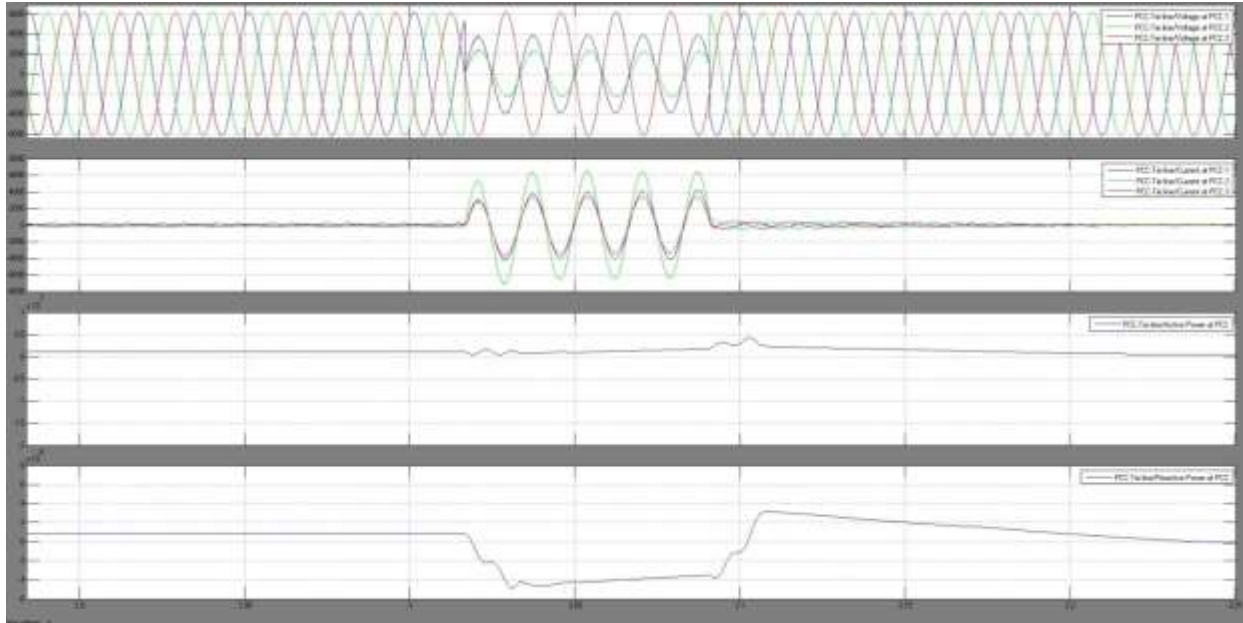
Figure 6.3. V, I, P and Q at PCC.

The voltage, current, active power and reactive power simulation results of battery are shown in the figure below. Battery current jumps from 12A to 4800A as shown in the figure. The voltage of two phases changes from 6000V to 2500V approximately. The reactive power supplied by the battery increases during the duration of fault and is contributes to being supplied to the main grid at PCC.

Figure 6.4.V, I, P and Q of Battery.

The voltage, current, active power and reactive power simulation results of PV are shown below. The current increases during the fault but gradually attains its normal case value.
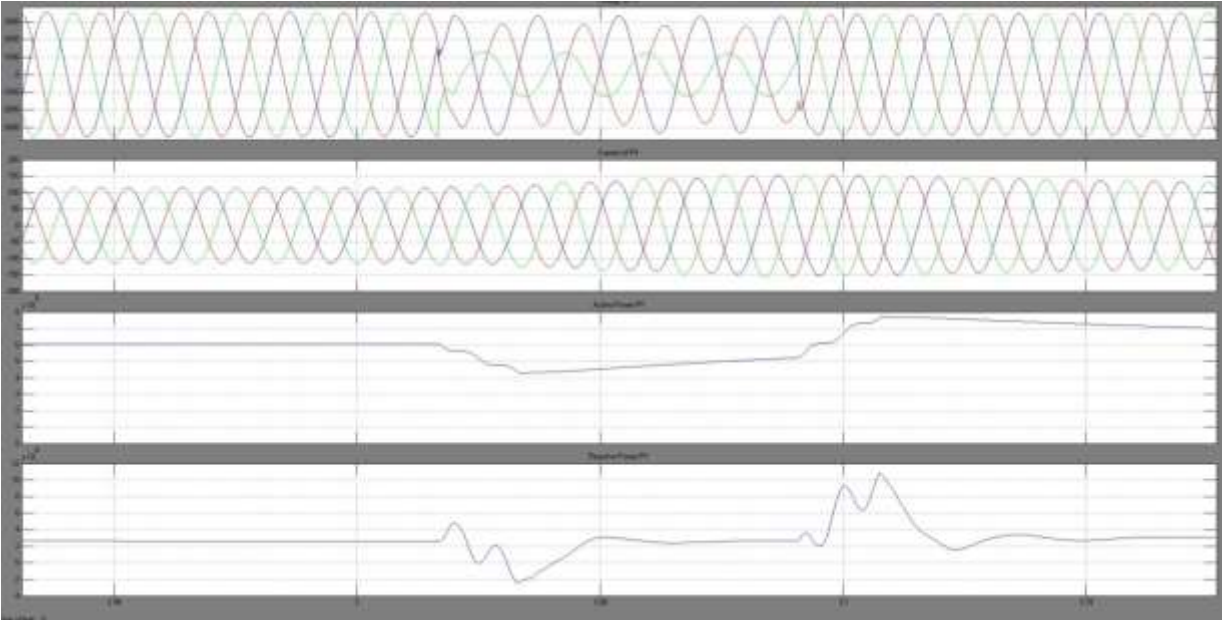
Figure 6.5. V, I, P and Q of PV.

The voltage, current, active power and reactive power simulation results of Diesel Generator are shown below. There is a huge increase in the current of one phase during the duration of fault. Also, the reactive power increases during the duration of fault and contributes to the reactive power being supplied during that interval to main grid.
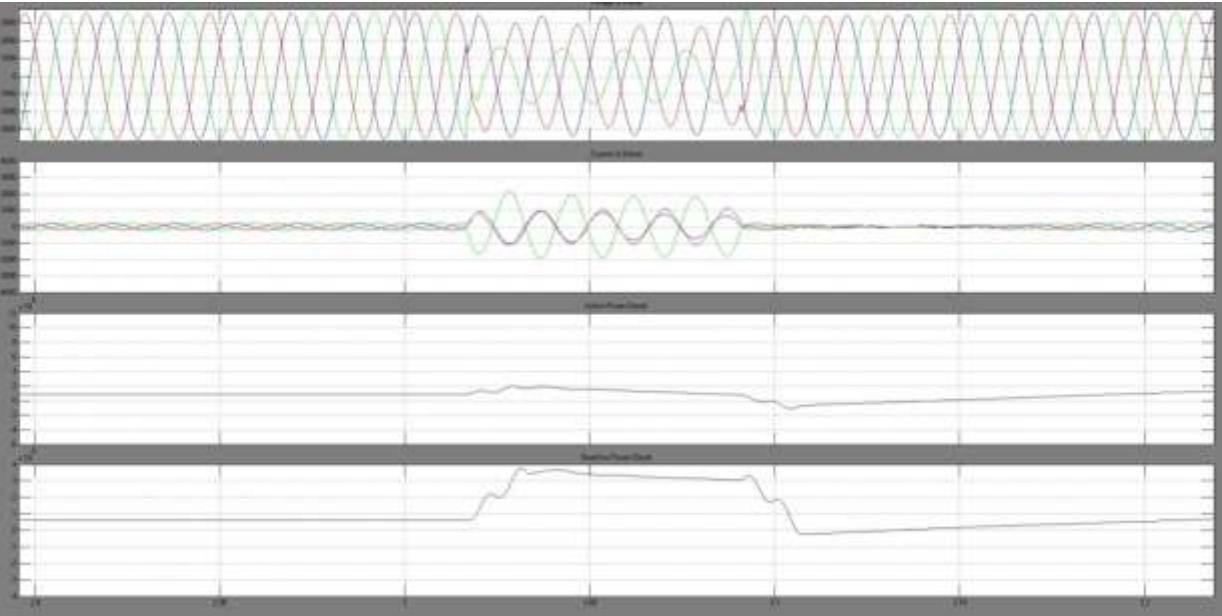
Figure 6.6. V, I, P and Q of Diesel Generator.

23

The frequencies at PCC, battery, PV and Diesel in the given order are shown below. The frequencies attain their stable value of 60Hz after the fault clear in about 0.5 seconds.

Figure 6.7. Frequencies at PCC, battery, PV and Diesel generator respectively.

2. Three-phase 4-cycles fault at Bus 632 near PV and PV is turned off during fault.

The 4-cycles three-phase fault is introduced at Bus 632 as shown in Figure 6.8.
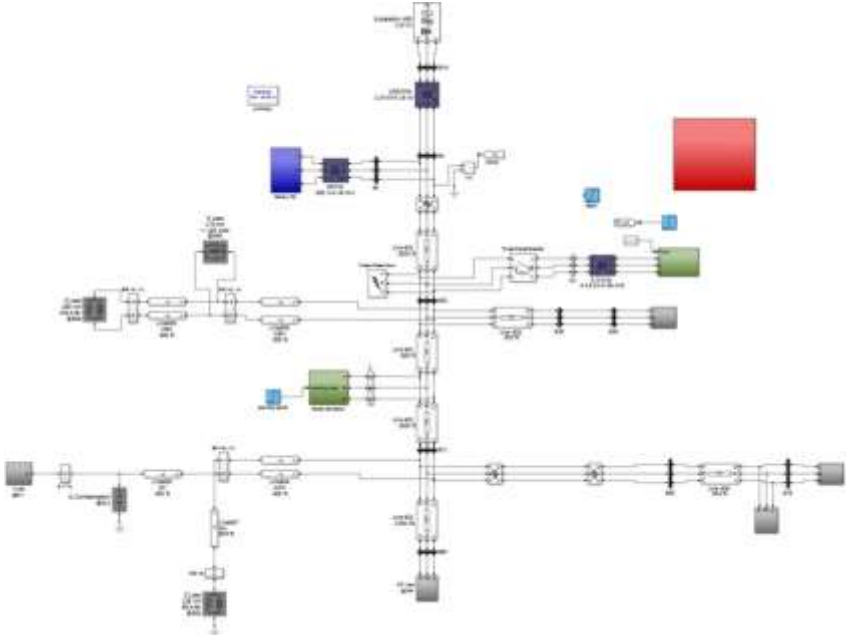
Figure 6.8. Three-phase 4-cycles fault at Bus 632 in Simulink model of Microgrid.

24

The voltage, current, active power and reactive power simulation results at PCC are shown in Figure 6.9. The flow of power is from microgrid to main grid at PCC. However, during the fault the active power flow reverses at PCC as shown below.

Figure 6.9. V, I, P and Q at PCC

The voltage, current, active power and reactive power simulation results of battery are shown in Figure 6.10.Battery being away from the point of three-phase fault is much less affected. The battery functions in its normal state except a sharp current peak at the time of fault.
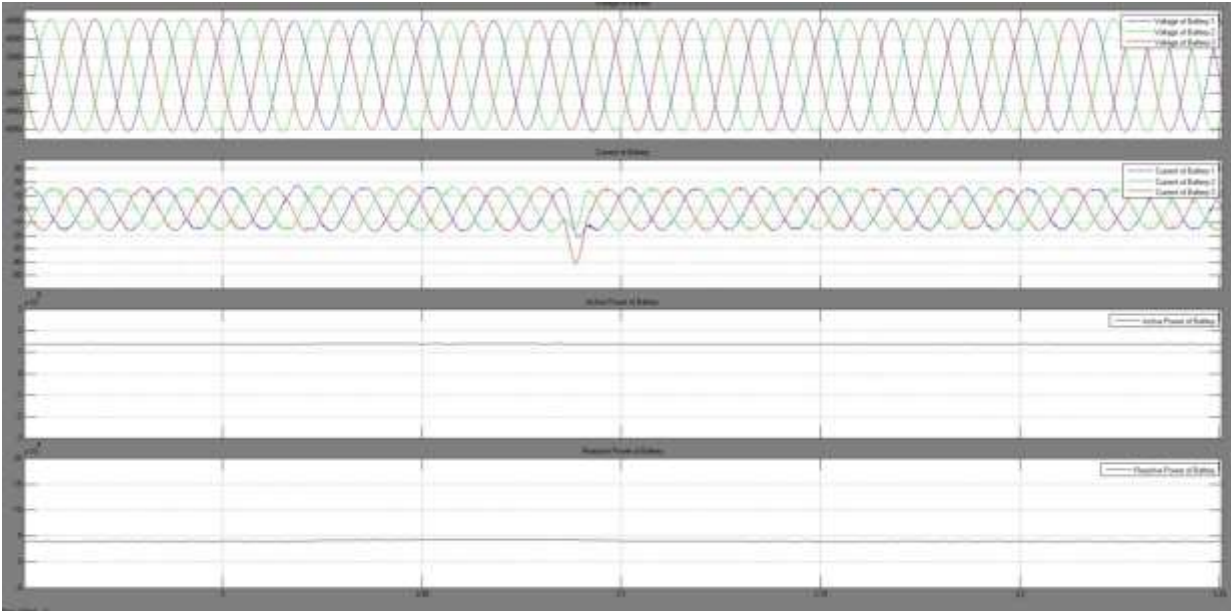
Figure 6.10. V, I, P and Q of Battery

The voltage, current, active power and reactive power simulation results of PV are shown below in Figure 6.11.During the fault, PV disconnects from the microgrid so the current and power drops to zero.
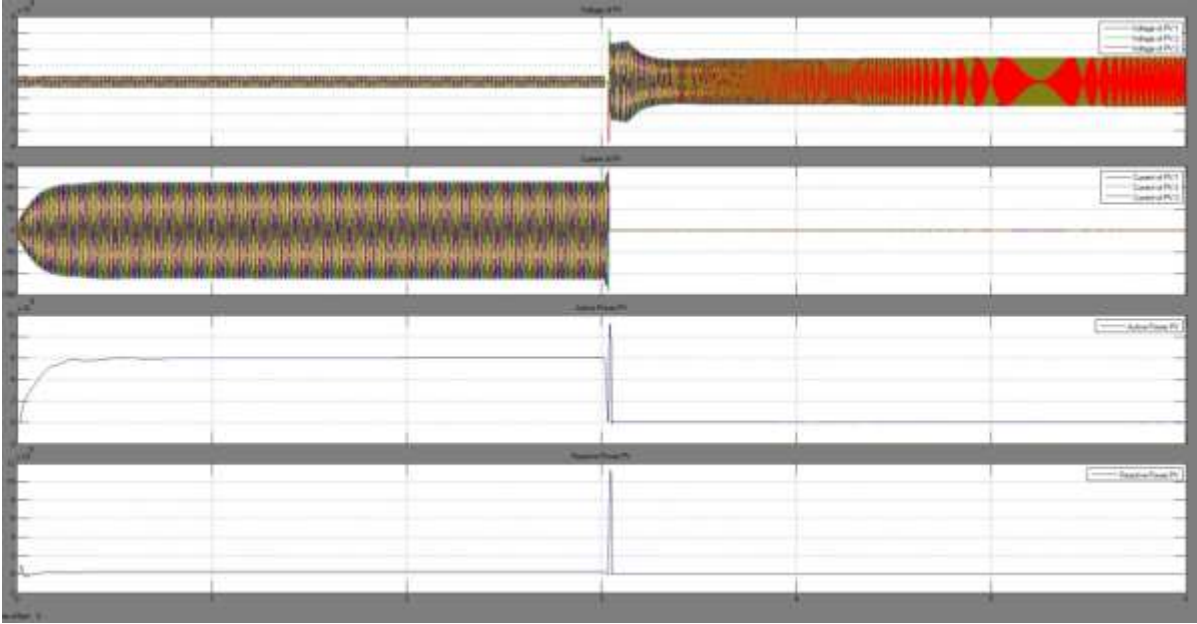
Figure 6.11. V, I, P and Q of PV.

The voltage, current, active power and reactive power simulation results of Diesel Generator are shown below. During the fault, the voltage drops to a lower value and current increases. There is some variation in the active and reactive power flow from the diesel generator and it does not attain its stable value even after the fault clears and become stable after about 0.3 seconds.

Figure 6.12. V, I, P and Q of Diesel Generator.

26

The frequencies at PCC, battery, PV and Diesel generator in the given order are shown below.The frequency of PV gets higher after disconnection but that is irrelevant as it won't be connected to the microgrid.The system is well synchronized at 60 Hz after the fault clears.
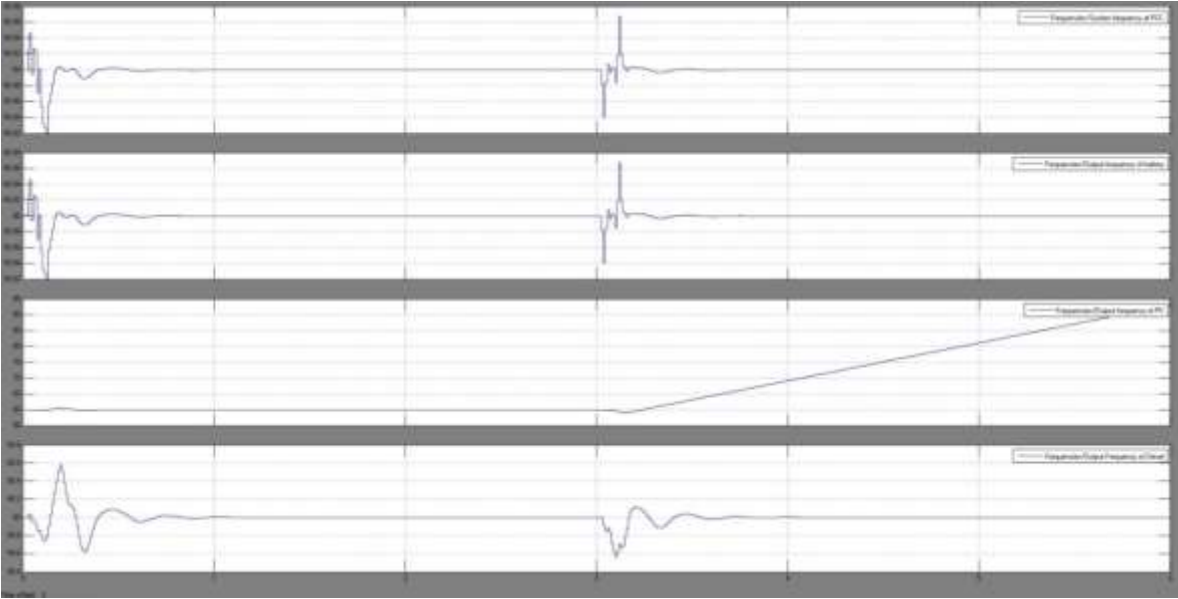
Figure 6.13. Frequencies at PCC, battery, PV and Diesel generator respectively.

3. *Sudden load decrease in microgrid*

The load in microgrid is decreased by cutting off two lines as shown in the figure below.
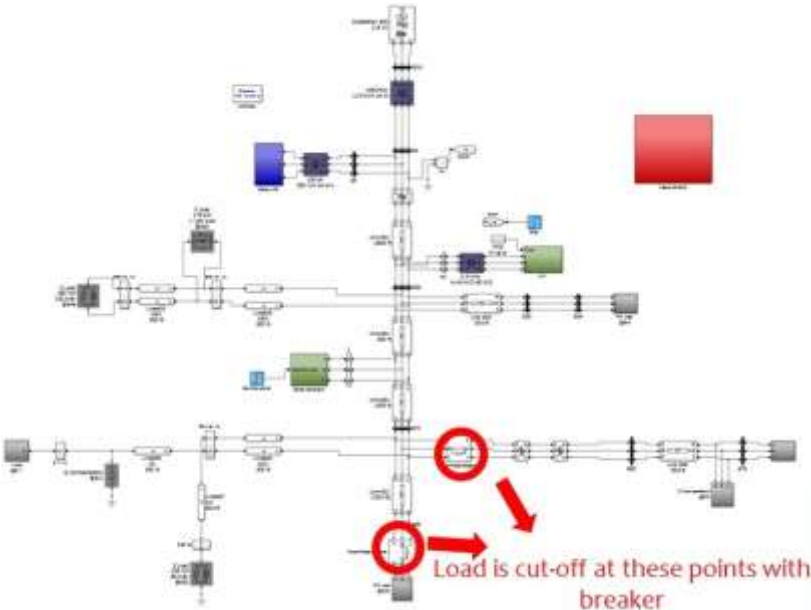
Figure 6.14. Sudden load decrease in microgrid.

The voltage, current, active power and reactive power simulation results at PCC are shown below. Initially, the active power is being supplied from main grid to microgrid but after the sudden decrease of load in microgrid, the flow of active power at PCC reverses. The reactive power flow from main grid to microgrid drops down after the sudden load decrease in microgrid. Also, the unbalance between the phases in the current at PCC increases after the load drop.
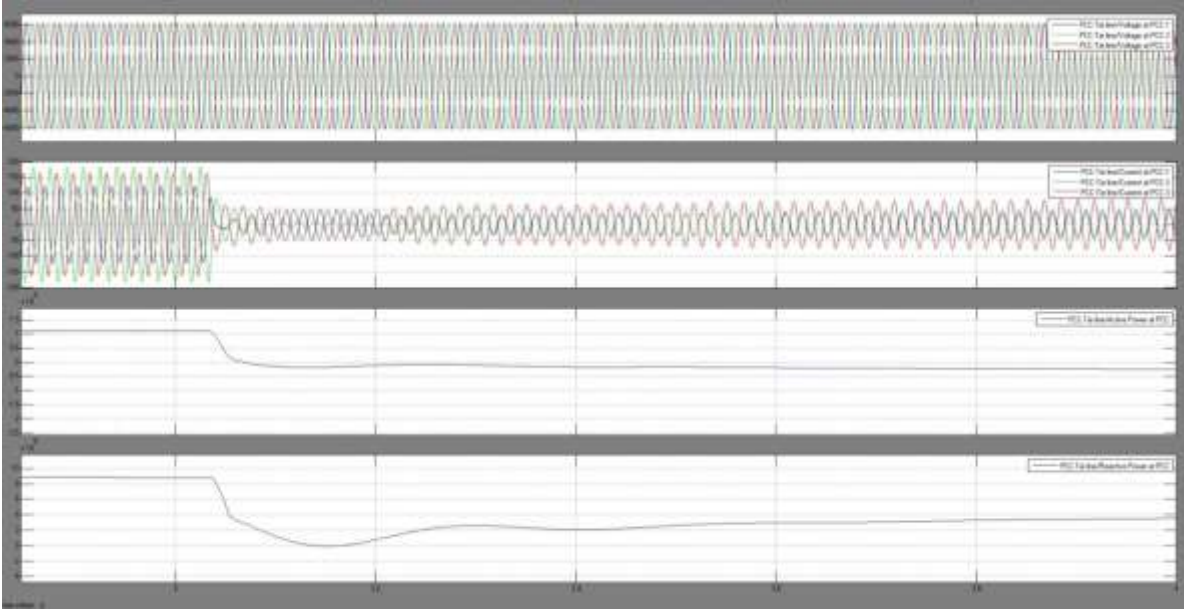
Figure 6.15. V, I, P and Q at PCC.

The voltage, current, active power and reactive power simulation results of battery are shown in Figure 6.16. Battery is of comparatively lower power capacity and therefore, the output of battery remains the same as before even after the load decrease.

Figure 6.16. V, I, P and Q of Battery.

28

The voltage, current, active power and reactive power simulation results of PV are shown below. The PV active power steps up after the load cuts off. The reactive power supplied by PV first increase for 0.2 seconds and then drops down.
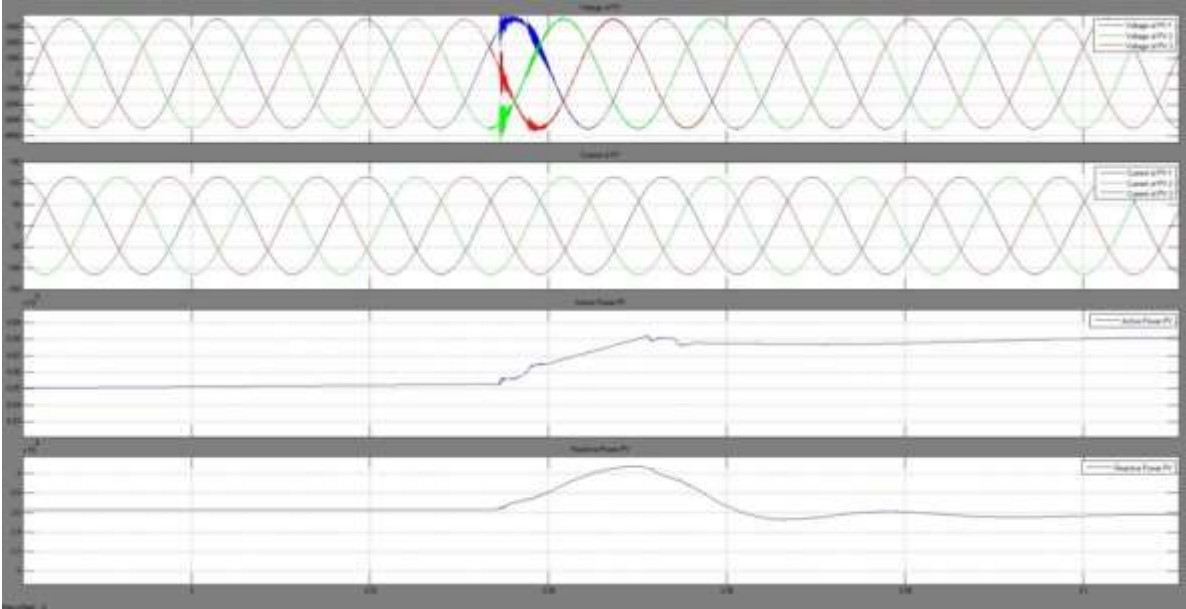
Figure 6.17. V, I, P and Q of PV.

The voltage, current, active power and reactive power simulation results of Diesel Generator are shown below. The reactive power supplied by diesel generator decreases after the load cuts off. There is some variation in the output of the diesel generator due to the sudden load decreases but it gradually become stable.
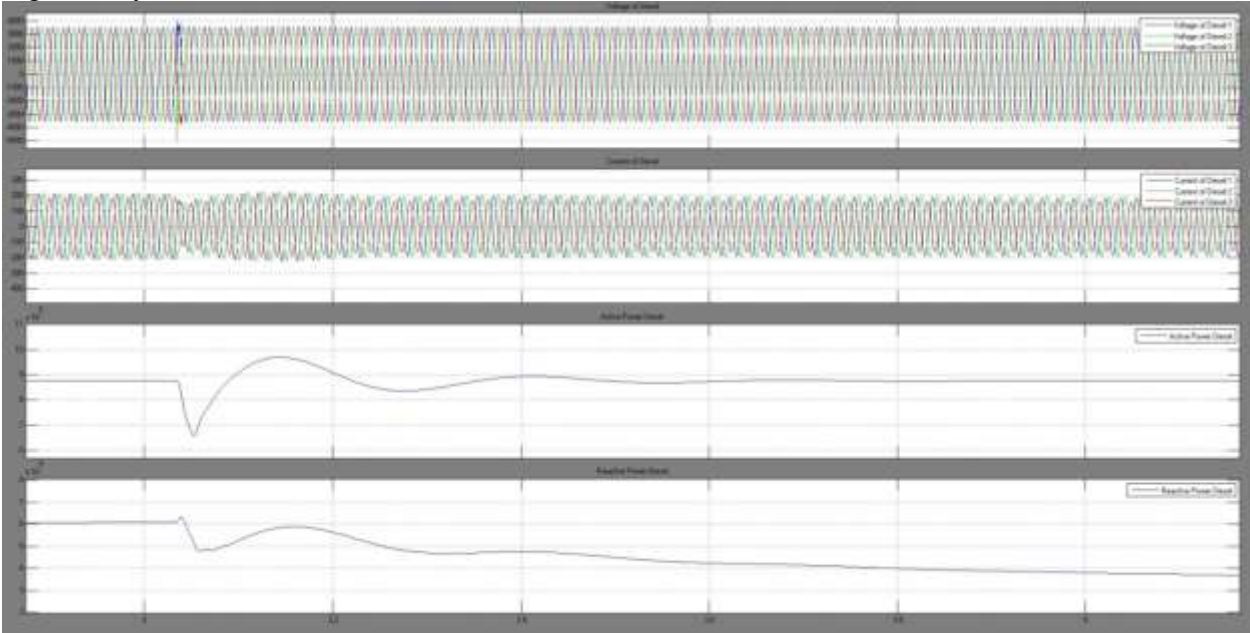
Figure 6.18. V, I, P and Q of Diesel Generator.

The frequencies at PCC, battery, PV and Diesel generator in the same order are shown below. The frequencies become stable at 60 Hz after 0.05 seconds.
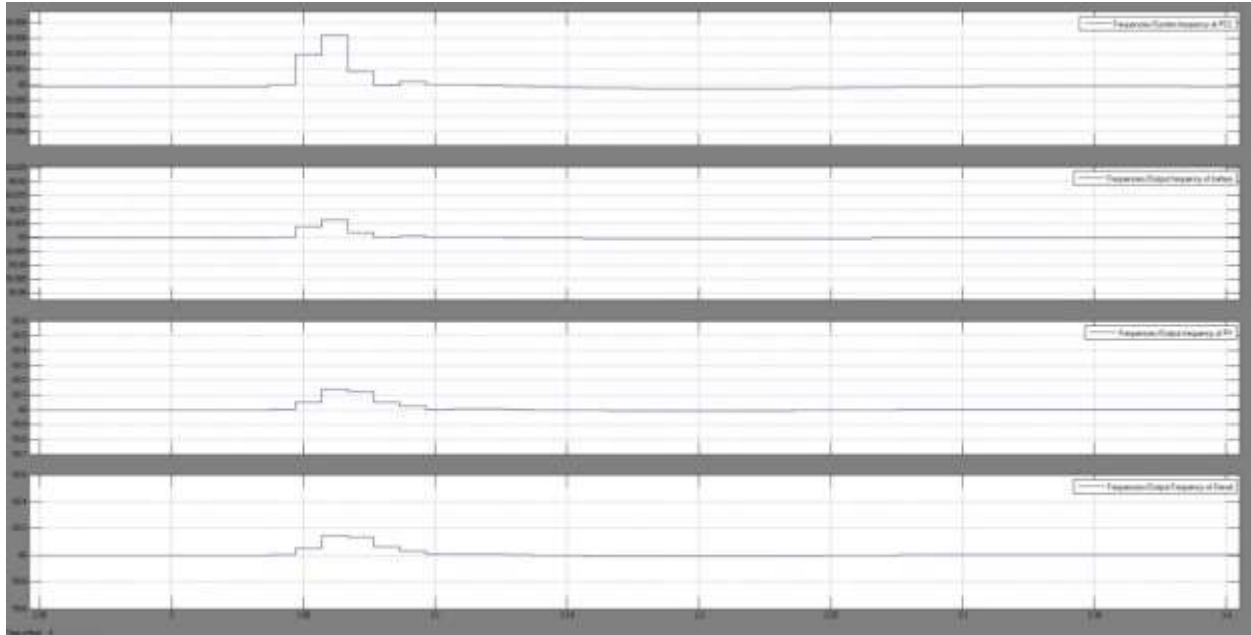
Figure 6.19. Frequencies at PCC, battery, PV and Diesel generator respectively.

Kundur's Two Area System

Kundur's Two Area System is then used to Kundur's two area system consists of two areas and 11 buses, connected by a weak tie between bus 7 and 9.The system operates at the fundamental frequency of 60 Hz. Each area consists of two generators, each having a rating of 900 MVA and 20 kV. The load in Area 1 is 967MW +100MVAR -187MVAR with the shunt capacitance of 200MVAR. The load in Area 1 is 1767MW + 100MVAR - 187MVAR with the shunt capacitance of 350MVAR. There is power flow of 413 MW from Area 1 to Area 2.
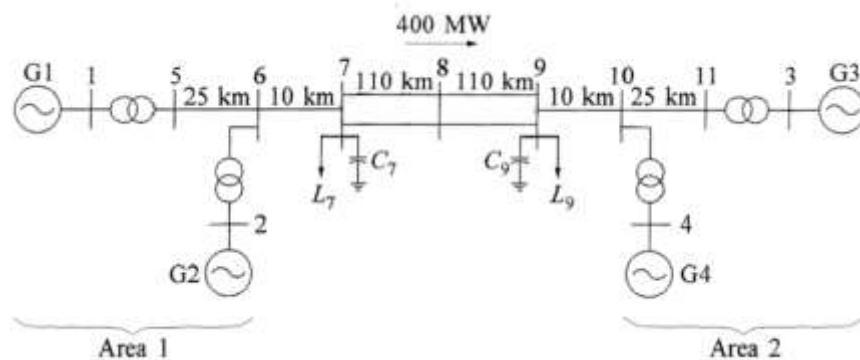
Figure 6.20. Tie-line diagram of Kundur's Two-Area System [21].

The Simulink model of this Kundur's Two-Area System is shown in Figure.6.20 (a),(b) and (c) below. The microgrid is in Area 2.
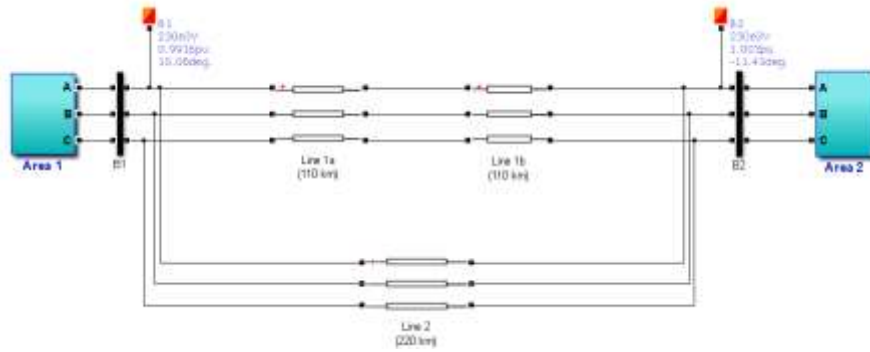
Figure 6.21(a) Simulink Model of Kundur's Two-Area System
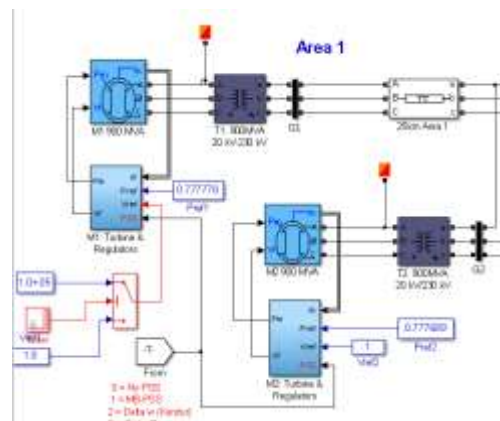
Figure6.21(b). Area 1 of Kundur's Two-Area System
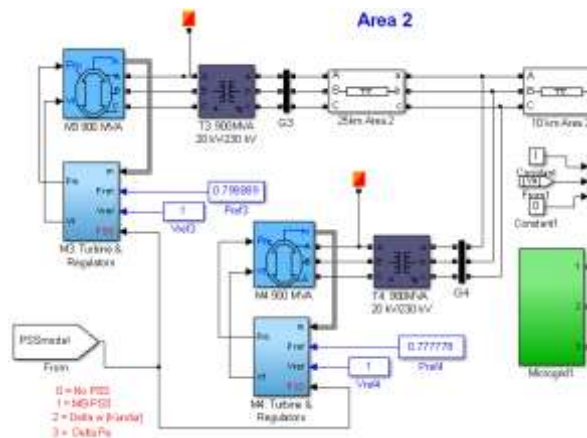
Figure.6.21(2). Area 2 of Kundur's Two-Area System

The following contingency simulation was done to analyze the behavior of the system when the microgrid is connected to the two-area system which emulates the behavior of generators in large-scale real power grid system.

Three phase 10-cycles fault in grid-mode at Bus 1 followed by islanding:

The results obtained by simulating a three phase 10-cycles fault at Bus 1 in the two area system shown in Figure 6.21(a) are given below.

In grid mode, active power at PCC is negative which means that grid is supplying power to microgrid. The three-phase measurement used at PCC in this simulation is in reverse direction compared to the one used in the previous simulations when an ideal voltage source was connected as a grid. After disconnection from grid, active power of diesel generator increases after islanding to provide for the load in microgrid as shown in figure 6.22.
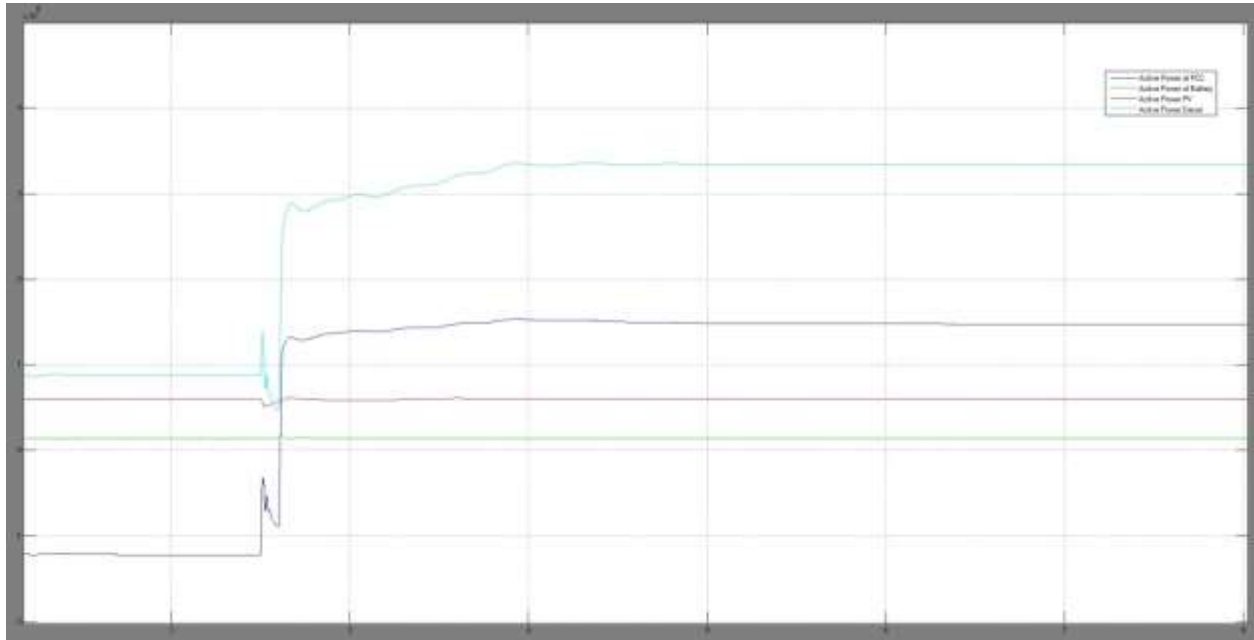
Figure 6.22. Active Power Flow at PCC, Battery, PV and Diesel Generator.

The reactive power of diesel generator increases after islanding, reactive power of PC increases for 0.5 seconds and then settles when reactive power of diesel generator starts providing the required reactive power in microgrid as shown in Figure 6.23.
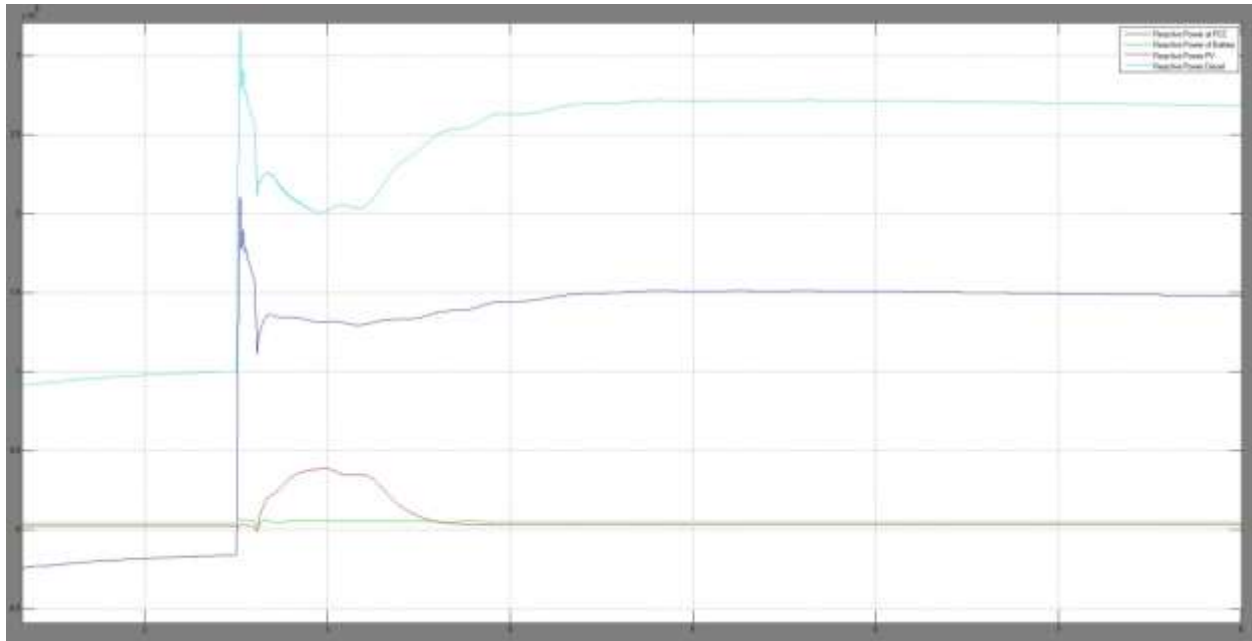
Figure 6.23. Reactive Power Flow at PCC, Battery, PV and Diesel Generator.

The frequencies of generators 1 and 2 closer to the fault location increases instantly after the fault compared to the generators in Area 2which are farther away from the point of fault as shown in figure below.
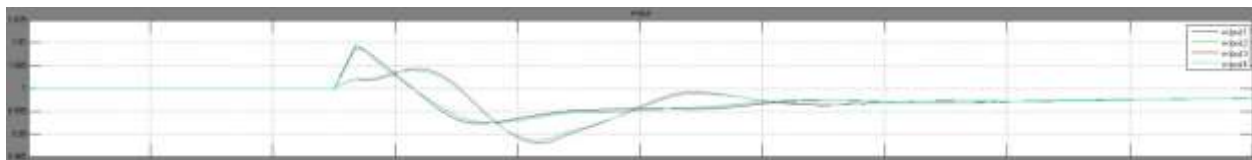
Figure 6.24. Frequencies of generators in Kundur's Two-Area System.

The frequencies of PCC, battery, PV and Diesel generator for this case of simulation are shown in Figure 6.25.The frequencies of all 3 DGs dips to 58.3 Hz during fault but gets stable after islanding.
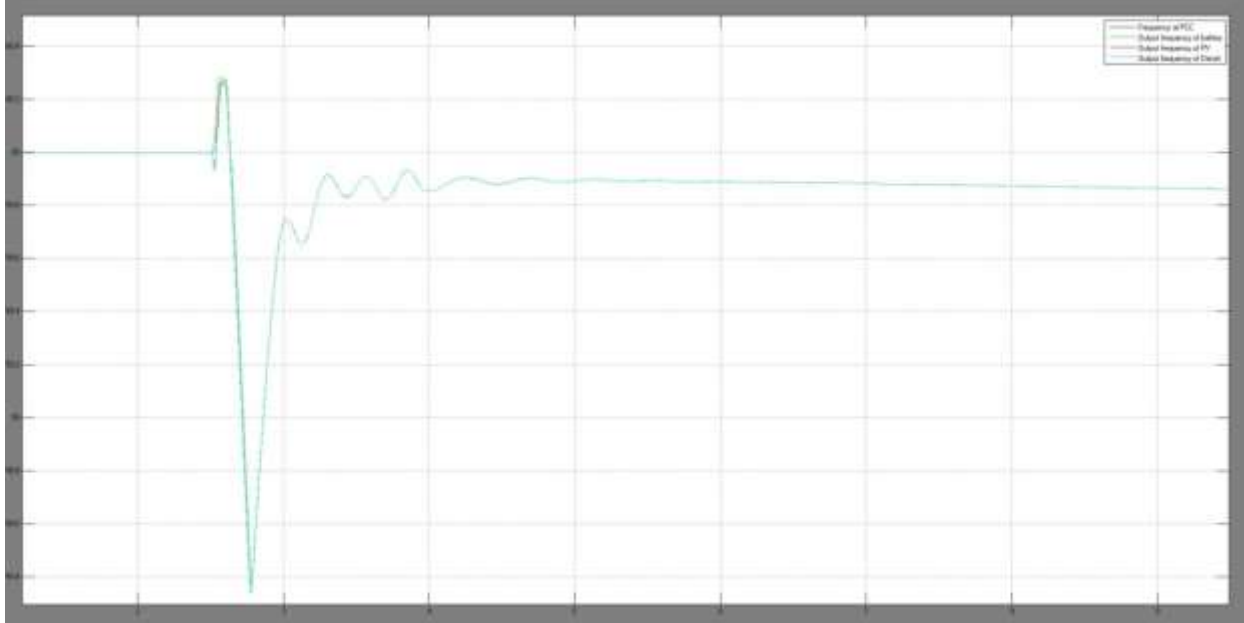
Figure 6.25. Frequencies at PCC, battery, PV and Diesel generator.

The voltage, current, active power and reactive power simulation results of battery are shown below. The reactive power output of the battery increases after islanding as shown. The voltage drops and the current increase because there is no power flow from main grid to microgrid and the distributed generators in microgrid provide for the load in microgrid.
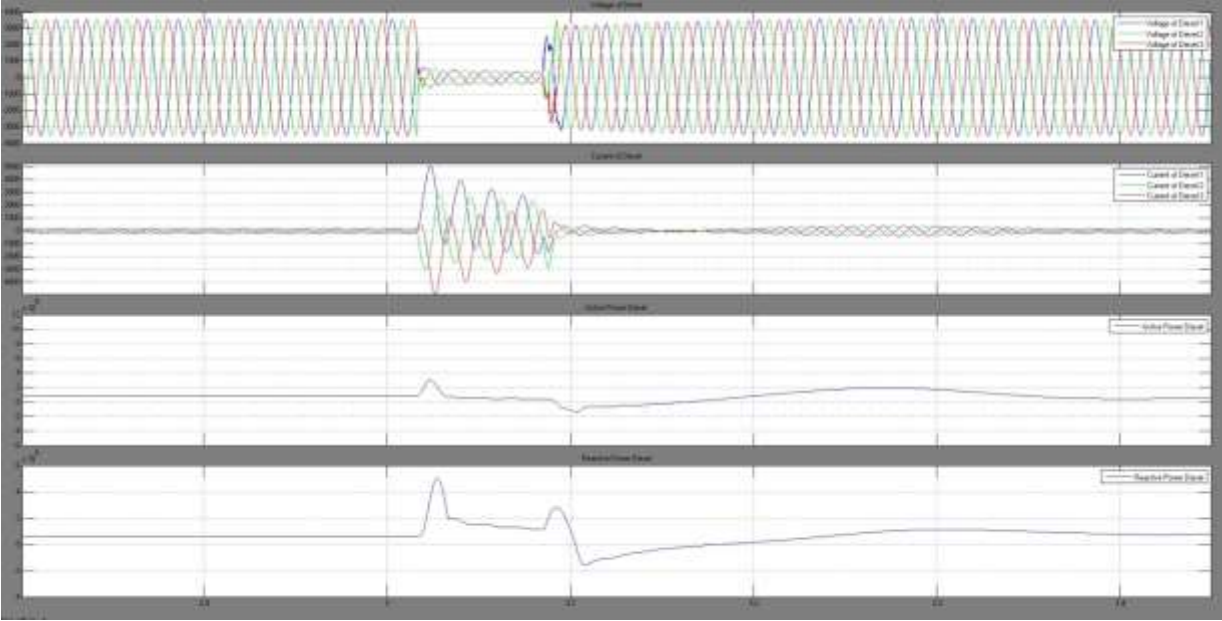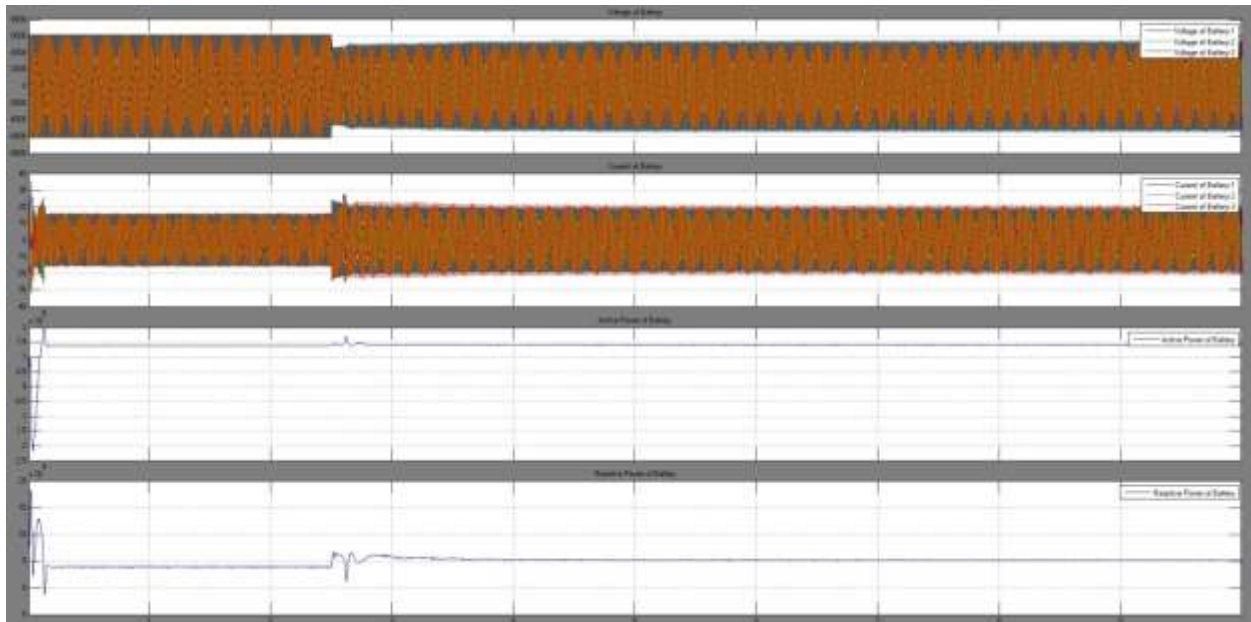

Figure 6.26. V, I, P and Q of Battery

34

The voltage, current, active power and reactive power simulation results of PV are shown below. The reactive power of PV increases after islanding to compensate the reactive load in the microgrid.
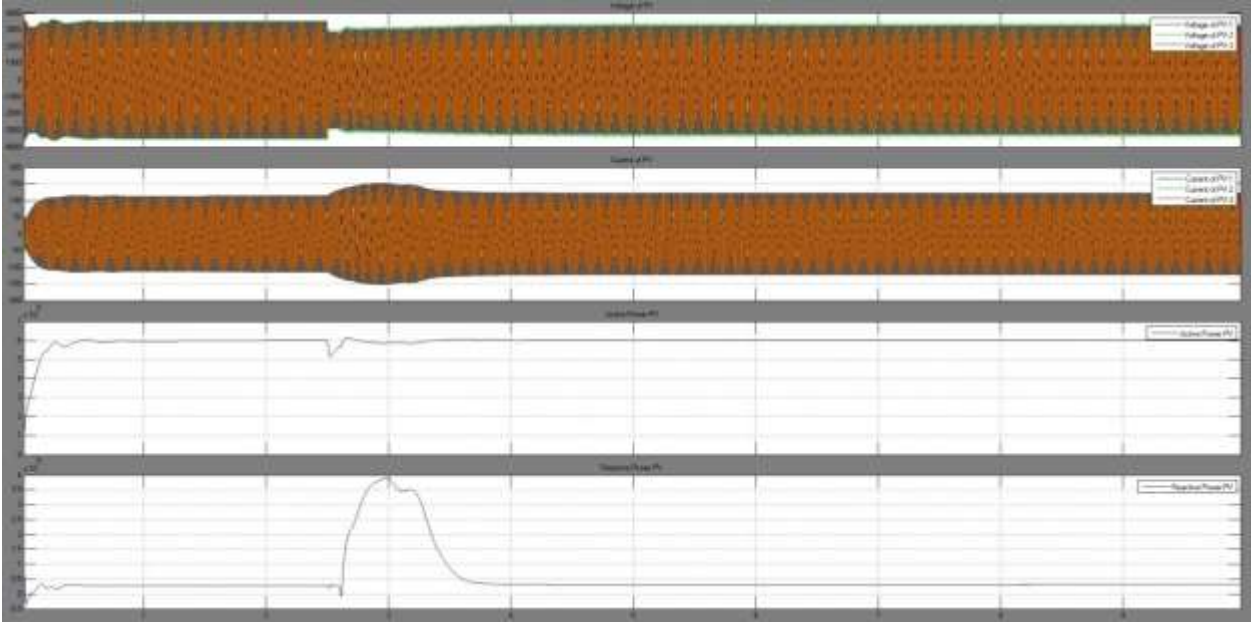
Figure 6.27. V, I, P and Q of PV

The voltage, current, active power and reactive power simulation results of diesel generator are shown below. The reactive power of diesel decreases for a short interval when reactive power of PV is providing the reactive power to the microgrid.
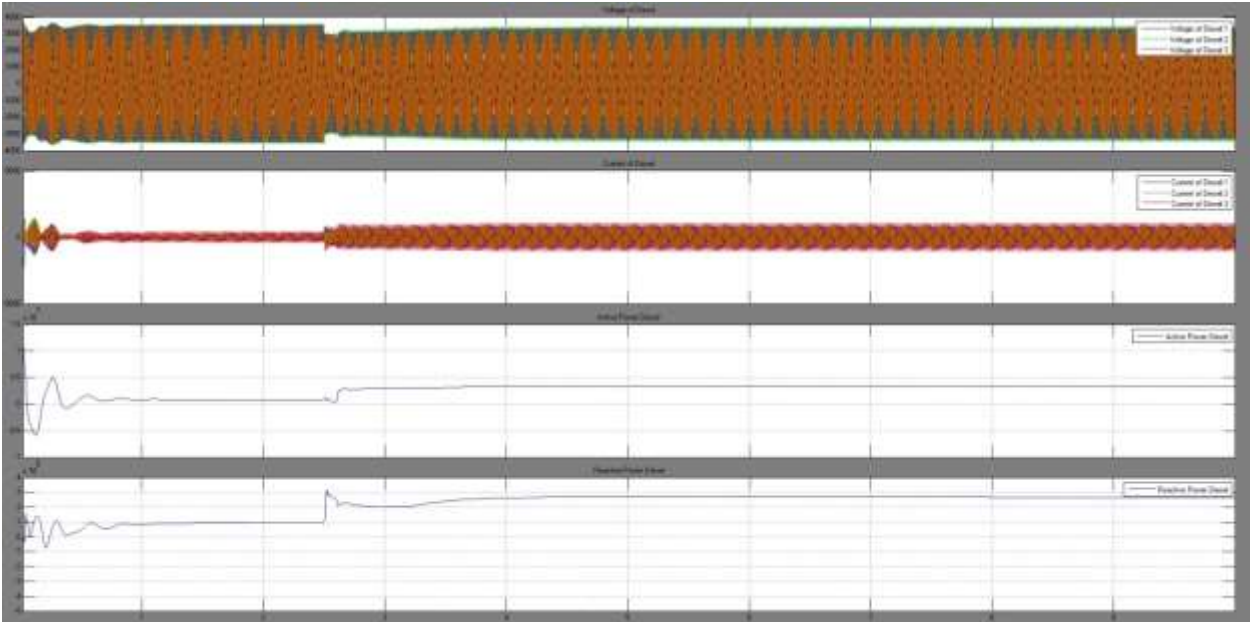
Figure 6.28. V, I, P and Q of Diesel Generator in microgrid.

CHAPTER 7 : DECISION TREES

Overview and Applications

Data mining (also known as knowledge discovery) is the process of detecting underlying correlations or patterns among different entities in large relational database. Data mining draws ideas from machine learning, artificial intelligence, pattern recognition. Several data mining techniques such as- Artificial Neural Networks, Decision Trees, Support Vector Machines and Bayesian Networks have been used in the field of power system data analytics. Among these data mining techniques, especially those with "white box" nature, such as artificial neural network, support vector machine etc., decision trees has gained increasing interests because it not only provides the insight information of data sets with low computational burden, but also reveals the principles learnt by DTs for further interpretation. Apart from these features, decision trees are better suited for managing the uncertainties associated with power systems through the use of statistical methods to increase the reliability [17]. The following sections presents a brief overview of decision tree based approaches in power system applications and provides an outline for the decision tree based decision making approach adopted in this project.

Decision trees (DTs) belong to a class of data mining tools capable of extracting useful information from large data set sand consequently provide assistance in decision-making processes. It is a supervised learning system with the objectives of classification and prediction similar to artificial neural networks and the group of other pattern recognition tools. In contrast to many other techniques, the general DT methodology builds classifiers in a hierarchical form, and selects automatically the most relevant features from among a (possibly large) list of candidates. The resulting classifiers (the decision trees) have forms compatiblewith typical human reasoning, which is easy to understand and interpret.

A DT-based method in general relies on three types of information: a learning set, composed of a samples of solved cases (i.e. cases pre-classified with respect to a given criterion), a list of critical attributes (i.e. of parameters likely to drive the phenomenaof concern, or in terms of which it is desirable to characterizesecurity), a DT building method which will select out of this listthe most relevant ones and formulate a security criterion in theform of a DT [18].

Decision trees have been previously used in electrical power system applications like- power system security assessment, fault diagnosis, protection, forecasting and identification etc. Fig.7.1 presents a simple five node decision tree for power system security assessment purpose where 'A' and 'B' are inputs to the decision tree, and the outcomes of the tree are classes "SECURE" and "INSECURE" [19].
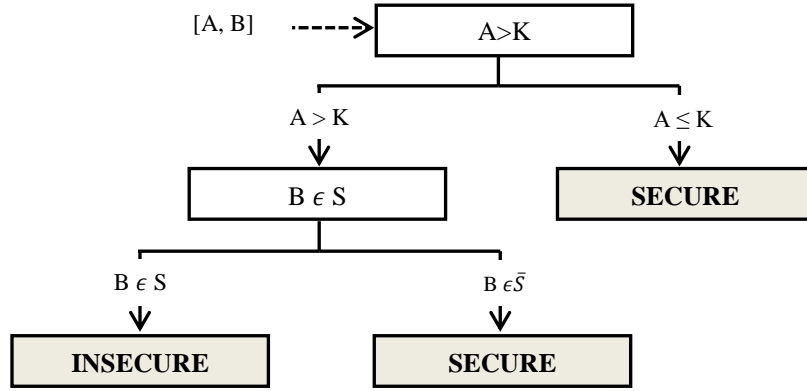
Figure 7.1. A simple 5 node decision tree [19]

A decision tree is made up of a set of nodes that uses supervised learning methods to achieve classification or prediction for an objective variable. As shown in Fig.7.1, a DT can predict the classification (e.g. "SECURE" or "INSECURE") of an object. The object is represented by a vector consisting of the values of a group of critical attributes (CAs, e.g. A and B in Fig.4.1). The classification process consists of dropping the vector of CAs down the DT starting at the root node until a terminal node is reached along a path, the class assigned to which is the classification result. At each inner (nonterminal) node, a question (i.e., a splitting rule) concerning a CA is asked to decide which child node the vector should drop into. For numerical variable A, the question compares it with a threshold; for categorical variable B, the question checks whether it belongs to a specified set.

Each of the elements (i.e. cases) in learning set and test set consists of a classification and a vector comprisingof the values of a group of CA candidates (called "predictors").The building process initially grows a maximal tree by recursively splitting a set of learning cases(i.e., a parent node) into two purer subsets (i.e., two new child nodes). To achieve each split, all possible splitting rules relatedto predictors are scored by how well different classes of casesin the parent node are separated. The splitting rule with the highest score isselected and called a "critical splitting rule" (CSR). The othersplitting rules are called "competitors". Some splitting rules that can completely mimic the action of the CSR are called "surrogates".Acompetitor with the same improvement score as that ofthe CSR can generate an equivalently good split and a surrogatecan generate exactly the same split as the CSR. The maximaltree is then pruned to generate a series of smaller DTs. The testset is used to test their performance. A commonly used index isthe misclassification cost, which is calculated using

$$R^{ts} = \frac{1}{N^{ts}}\sum_{i,j} c(i|j).N_{ij}^{ts} \qquad (7.1)$$

where, N^{ts} is the number of test cases, $c(i|j)$ is the cost of misclassifying a class j case as a class i case and N_{ij}^{ts} is the number of class j cases whose predicted class is i. The correctness rate of classifying class i cases is denoted by CR_i^{ts}

$$CR_i^{ts} = \left(N_{ii}^{ts} \big/ N_i^{ts} \right).100\% \qquad (7.2)$$

37

where, N_i^{ts} is the number of class i test cases. For a sufficient number of test cases, a smaller R^{ts} generally corresponds to a better decision tree. If statistical errors are also considered, the standard error estimate for R^{ts} is denoted as ΔR^{ts} and is calculated as following,

$$\Delta R^{ts} = [R^{ts}(1 - R^{ts})/N^{ts}]^{1/2} \qquad (7.3)$$

Two decision trees whose cost difference is smaller than the standard error estimate of either one have almost equal performance [19-20].

This project proposes a Decision Tree (DT) based approach for assisting microgrid central controller in the decision making tasks under the following circumstances:

- Islanding decision processes following a grid side contingency while the microgrid is working in grid-connected mode.
- Preventive and corrective control decision processes following contingencies within microgrid while the microgrid system is working in islanding mode.

In this project, each of the above mentioned tasks are realized using the following steps:

- *Offline Contingency Database Preparation*: A contingency database is prepared using simulations studies performed on the microgrid model by recording all of the potential critical attributes (CAs) and an offline classification. These databases are used to train the decision trees.
- *Decision Tree Training*: Decision trees are trained using the offline contingency databases prepared in the previous step. Then the DTs are allowed to identify the critical attributes (CAs) that characterize the decision criteria in the best possible way.
- *DT Testing and Performance Assessment*: Test data sets for testing the trained DTs are generated and performances of the decision trees are evaluated using the accuracy of the classification.
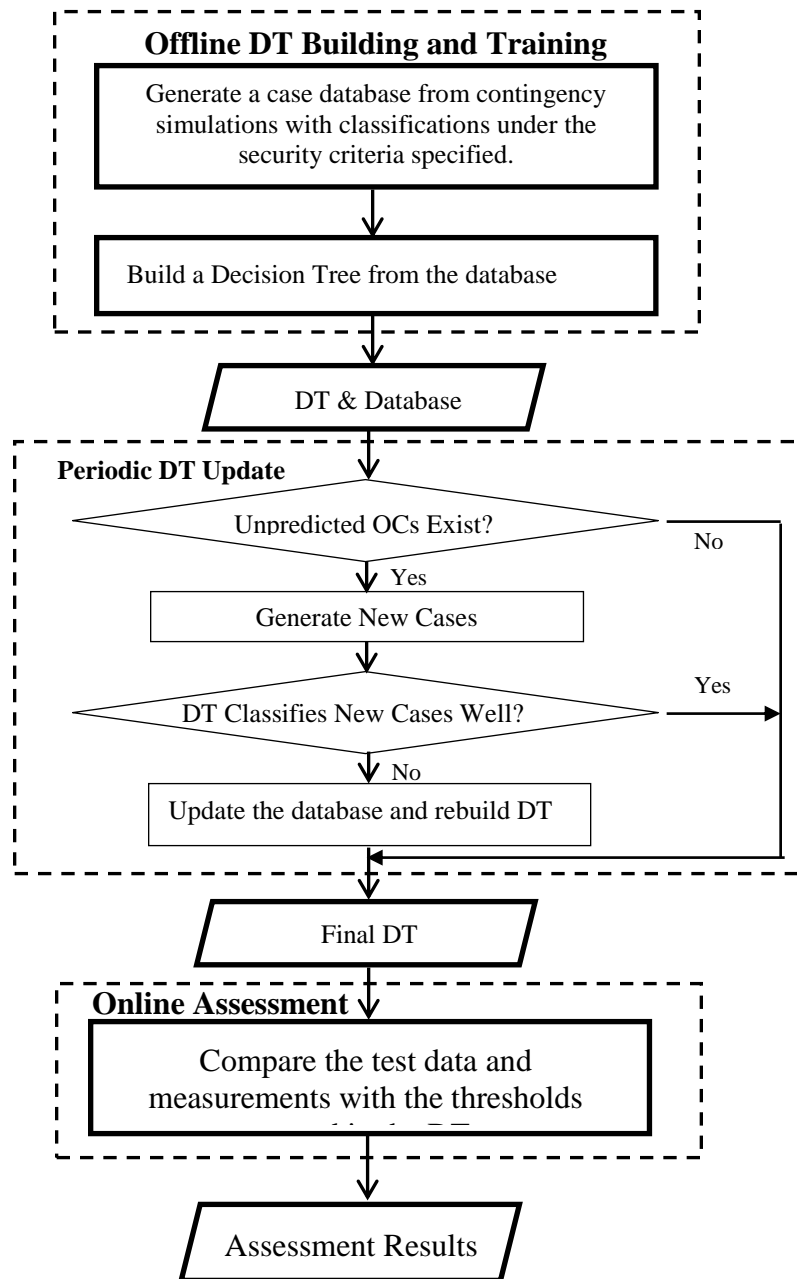
Fig.7.2. DT based scheme for microgrid islanding and controls

In the above mentioned procedure, each DT is built using J48 decision tree algorithm which is the Java version of the popular C4.5 decision tree algorithm. Fig.7.2 presents the conceptual flowchart for the decision tree building approach used in this project from database generation, training and testing phases.

Decision Tree for Microgrid Islanding Assistance

Security Criteria, Implementation Methodology, Test Results

The ever increasing data availability in modern power systems prompts the application of data mining tools for power system data analysis. Prominent data mining techniques like decision tree have been utilized for power system security assessment, preventive and corrective controls, fault diagnosis, protection, forecasting and identification. This project intends to utilize decision trees in assisting microgrid central controller in islanding decision making while working in the grid connected mode as well as in providing assistance in preventive and corrective control decisions while working in the islanding mode.

Microgrid central controller is required to island the system from main grid following system contingencies that violates the standard interconnection requirements for distributed energy resources set by IEEE Standard 1547. According to IEEE 1547, the islanding decisions while in grid connected mode are predominantly based on system voltage and frequency measurements at point of common coupling. Decision trees can be trained and implemented to detect underlying patterns and relationships among various system variables that can be used for predicting system voltages and frequency following contingencies for assisting the islanding decision process.

 The following subsections provide a brief overview of the islanding decision criteria based on system voltage and frequency requirements from IEEE 1547 and summarizes the implementation of decision trees for assistance in islanding decision including the event database creation, data preprocessing, tree structures and preliminary results.

Review of IEEE 1547 Requirements on Voltage

The protection functions of the interconnection system shall detect the effective (RMS) or fundamental frequency value of each phase-to-phase voltage, except where the transformer connecting the DR to the Area EPS is a grounded wye-wye configuration, or single-phase installation, the phase-to-neutral voltage shall be detected. When any voltage is in a range given in Table.4.2, the DR shall cease to energize the Area EPS within the clearing time as indicated. Clearing time is the time between the start of the abnormal condition and the DR ceasing to energize the Area EPS. For DR less than or equal to 30 kW in peak capacity, the voltage set points and clearing times shall be either fixed or field adjustable. For DR greater than 30 kW, the voltage set points shall be field adjustable [15].

The voltages shall be detected at either the PCC or the point of DR connection when any of the following conditions exist:

      1. The aggregate capacity of DR systems connected to a single PCC is less than or equal to 30 kW.
      2. The interconnection equipment is certified to pass a non-islanding test for the system to which it is to be connected.
      3. The aggregate DR capacity is less than 50% of the total Local EPS minimum annual integrated electrical demand for a 15-minute time period, and export of real or reactive power by the DR to the Area EPS is not permitted [15].

Table 7.1. Interconnection System Response to Abnormal Voltages [15]

Voltage Range [% of base voltage]	Clearing time [sec]
V < 50	0.16
50 ≤ V < 88	2.00
110 ≤ V < 120	1.00
V ≥ 120	0.16

Review of IEEE 1547 Requirements on Frequency:

When the system frequency is in a range given in Table 4.3, the DR shall cease to energize the Area EPS within the clearing time as indicated. Clearing time is the time between the start of the abnormal condition and the DR ceasing to energize the Area EPS. For DR less than or equal to 30 kW in peak capacity, the frequency set points and clearing times shall be either fixed or field adjustable. For DR greater than 30 kW the frequency set points shall be field adjustable. Adjustable under frequency trip settings shall be coordinated with Area EPS operations [15].

Table 7.2. Interconnection System Response to Abnormal Frequencies [15]

DR Capacity	Frequency Range [Hz]	Clearing Time [sec]
≤ 30 KW	>60.5	0.16
	<59.3	0.16
>30KW	>60.5	0.16
	>57 and <59.8 Adjustable set point	Adjustable 0.16 to 300
	<57.0	0.16

Data Preprocessing and Decision Tree Training:

Decision trees are trained using contingency databases created from fault simulations on the grid side in the simulation model. The simulation model consists of a two area electrical power system with the microgrid connected in bus B2 in area-2 of the system. Two contingency databases have been created with identical grid side fault simulation scenarios for classification of voltage and frequency abnormalities. Each of these databases contain 48 cases generated from 6 buses from Area-1 and Area-2 under 4 different types of faults and two different system loading scenarios.

The training data set for decision trees have been preprocessed to include the potential critical attributes that can characterize and predict the events related to voltage and frequency abnormalities as well as sample voltage and frequency classifications have been generated for the supervised training of the decision trees.

The events associated with voltage and frequency abnormalities mentioned in IEEE Standard 1547 are classified into five subcategories for voltage related events and four subcategories for

frequency related events. Based on these classification results, each of the fault simulation cases have been labeled with frequency and voltage classes which have been used to train the decision tree. Table 7.3 and Table 7.4 present the voltage and frequency classes along with the IEEE 1547 standards respectively.

Table 7.3. Interconnection System Response to Abnormal Voltages with Class Identifier

Voltage Range [% of base voltage]	Clearing time [sec]	Class Identifier
V < 50	0.16	VU2
50 ≤ V < 88	2.00	VU1
88 ≤ V < 110	-	VN
110 ≤ V < 120	1.00	VO1
V ≥ 120	0.16	VO2

Table 7.4. Interconnection System Response to Abnormal Frequencies with Class Identifier

DR Capacity	Frequency Range [Hz]	Clearing Time [sec]	Class Identifier
≤ 30 KW	>60.5	0.16	FO1
	59.8< f < 60.5	-	FN
	<59.3	0.16	FU1
>30KW	>60.5	0.16	FO1
	59.8< f < 60.5	-	FN
	>57 and <59.8 Adjustable set point	Adjustable 0.16 to 300	FU1
	<57.0	0.16	FU2

Table 7.5 lists the critical attributes used in developing the decision trees for voltage and frequency classification purpose in order to assist in the islanding decision process. The list includes voltage, current, frequency, real and reactive power values. In addition to those system parameters, a series of abnormal voltage and frequency event identifiers have also been included in the list. The elements in the critical attribute list have been chosen keeping in mind the possibility of losing a certain type of measurements (i.e. voltage measurements) and yet being able to predict and classify the incoming voltage and frequency abnormalities. The voltage and frequency events identifier included in the list can be utilized not only to detect the abnormal events but also they can be utilized in detecting the sequence of the different classes of voltage and frequency abnormalities resulting from the same grid side contingency.

Table 7.6 and Table 7.7represents the preprocessed training data for decision tree training for frequency and voltage classification problems respectively. Table 7.8 and 7.9 presents the ranking of the predictors for the classification tasks. The ranking is obtained by removing the best ranked predictor from the training dataset in each of the previous iterations during the training process and allowing the decision tree algorithm to select the most suitable and relevant predictor in the current iteration. The corresponding accuracies are obtained under four different

42

test scenarios. The first sets of accuracies are obtained using the training data as the testing dataset. The second set of accuracies are obtained using the 10 folds "Cross-Validation" approach which basically divides the entire dataset into 10 individual pieces, and uses one of the pieces for testing the decision tree and the remaining nine pieces are used for training the decision tree. In this way the algorithm performs 11 iterations with each of the pieces in the dataset is used at least once as the testing data in the first 10 iterations and in the final iteration the entire dataset is treated as the testing data. From each of the iterations, accuracies are calculated and their average is computed which is the final accuracy result. This approach provides somewhat more realistic accuracy results compared to using the training dataset for testing the decision trees. The third and fourth set of accuracies are computed using 66% of the training dataset to train the tree and the remaining 34% to test the decision tree, and with 85% of the training dataset to train the tree and the remaining 15% of the dataset to test the decision tree respectively.

Table 7.5. List of critical attributes selected for building the decision trees

Critical Attribute	Category	Unit	Description
Fault Type(3p/1p)	Nominal	-	Type of the fault on the grid side
Location	Nominal	-	Location of the fault (Bus Number)
Area	Nominal	-	Area of the Faulted Bus
Vamin	Numeric	kV (rms)	Minimum phase-neutral voltage in phase-A
Vamax	Numeric	kV (rms)	Maximum phase-neutral voltage in phase-A
Vbmin	Numeric	kV (rms)	Minimum phase-neutral voltage in phase-B
Vbmax	Numeric	kV (rms)	Maximum phase-neutral voltage in phase-B
Vcmin	Numeric	kV (rms)	Minimum phase-neutral voltage in phase-C
Vcmax	Numeric	kV (rms)	Maximum phase-neutral voltage in phase-C
Iamin	Numeric	A (rms)	Minimum phase current in phase-A
Iamax	Numeric	A (rms)	Maximum phase current in phase-A
Ibmin	Numeric	A (rms)	Minimum phase current in phase-B
Ibmax	Numeric	A (rms)	Maximum phase current in phase-B
Icmin	Numeric	A (rms)	Minimum phase current in phase-C
Icmax	Numeric	A (rms)	Maximum phase current in phase-C
Pmin	Numeric	MW	Minimum real power
Pmax	Numeric	MW	Maximum real power
Qmin	Numeric	MVAR	Minimum real power
Qmax	Numeric	MVAR	Maximum real power
Fmin	Numeric	Hz	Minimum frequency
Fmax	Numeric	Hz	Maximum frequency
VU2a	Numeric	-	Class identifier
VU1a	Numeric	-	Class identifier
VO1a	Numeric	-	Class identifier
VO2a	Numeric	-	Class identifier
VU2b	Numeric	-	Class identifier
VU1b	Numeric	-	Class identifier
VO1b	Numeric	-	Class identifier
VO2b	Numeric	-	Class identifier
VU2c	Numeric	-	Class identifier
VU1c	Numeric	-	Class identifier
VO1c	Numeric	-	Class identifier
VO2c	Numeric	-	Class identifier
FO1	Numeric	-	Class identifier
FU1	Numeric	-	Class identifier
FU2	Numeric	-	Class identifier

Table 7.6. Decision tree Training Data for Frequency Classification Problem

No.	Class F Nominal	Fault Type (3p/1p) Nominal	Location Nominal	Area Nominal	Vamin Numeric	Vamax Numeric	Vbmin Numeric	Vbmax Numeric	Vcmin Numeric	Vcmax Numeric	Iamin Numeric	Iamax Numeric	Ibmin Numeric	Ibmax Numeric	Icmin Numeric	Icmax Numeric	Pmin Numeric	Pmax Numeric	Qmin Numeric	Qmax Numeric	Fmin Numeric	Fmax Numeric
1	FU	3-Phase	G3	Area-2	63449...	15526...	63804...	15446...	63718...	15489...	-3658...	383.3...	-1882...	1281...	418.4...	3351...	1.332...	6.625...	-8.709...	1.967...	59.35...	60.45...
2	FU	3-Phase	G4	Area-2	10197...	15704...	10256...	15668...	10208...	15718...	-2865...	574.2...	-1871...	2535...	-1621...	2657...	1.691...	6.196...	-5.341...	2.133...	59.28...	60.43...
3	FN	1-Phase-A	G3	Area-2	80873...	15078...	12199...	15055...	12176...	15052...	-1396...	343.5...	-1970...	-120.3...	730.8...	3144...	2.673...	6.404...	-6.163...	1.005...	59.63...	60.22...
4	FN	1-Phase-A	G4	Area-2	12105...	15390...	12149...	15364...	24848...	15367...	-2666...	321.3...	-1648...	685.6...	728.5...	3009...	2.198...	6.293...	-6.321...	1.725...	59.52...	60.30...
5	FN	1-Phase-B	G3	Area-2	12119...	15073...	81100...	15050...	12120...	15049...	-1317...	345.8...	-2045...	-215.9...	680.6...	3181...	2.625...	6.434...	-6.363...	1.030...	59.62...	60.23...
6	FN	1-Phase-B	G4	Area-2	12048...	15449...	24961...	15421...	12081...	15426...	-2778...	336.8...	-1682...	695.8...	634.4...	3082...	2.196...	6.333...	-6.667...	1.725...	59.51...	60.30...
7	FN	1-Phase-C	G3	Area-2	12178...	15035...	12200...	15012...	81059...	15011...	-1290...	332.9...	-2000...	-192.2...	707.8...	3105...	2.647...	6.399...	-6.083...	1.024...	59.64...	60.23...
8	FN	1-Phase-C	G4	Area-2	24869...	15344...	12193...	15318...	12184...	15320...	-2607...	300.9...	-1618...	720.8...	735.9...	2933...	2.242...	6.264...	-6.062...	1.710...	59.54...	60.29...
9	FU	3-Phase	B1	Area 0	2487...	17467...	6404...	20479...	4073...	18578...	-1955...	2663...	-2887...	1264...	-3322...	1814...	-6.022...	7.712...	-5.714...	1.188...	59.37...	60.3748
10	FU	3-Phase	B2	Area 0	4.504...	18414...	6.964...	22343...	11.46...	20794...	-2655...	2613...	-1776...	6144...	-2742...	2356...	-9.114...	6.178...	-4.849...	9.407...	59.27...	60.75...
11	FN	1-Phase-A	B1	Area 0	25647...	18496...	1169...	15555...	63102...	18891...	-1713...	1452...	-1934...	636.6...	-2408...	-1014...	6.356...	5.326...	-2.618...	1.334...	59.79...	60.08...
12	FN	1-Phase-A	B2	Area 0	16.04...	19205...	2781...	17618...	88812...	21963...	-1714...	6618...	-1584...	431.2...	-2716...	-814.6...	-3.640...	5.820...	-4.567...	-7.184...	59.66...	60.17...
13	FN	1-Phase-B	B1	Area 0	24731...	18185...	1590...	15628...	50423...	18901...	-1748...	328.7...	-1812...	752.6...	-2340...	-917.4...	4.720...	5.397...	-2.629...	1.431...	59.78...	60.07...
14	FN	1-Phase-B	B2	Area 0	4333...	19303...	8.336...	18105...	83542...	20465...	-1807...	330.0...	-1614...	3222...	-2742...	-663.2...	-3.662...	5.929...	-4.547...	-7.328...	59.65...	60.17...
15	FN	1-Phase-C	B1	Area 0	21251...	18475...	1666...	15580...	62555...	18884...	-1717...	813.2...	-1741...	644.6...	-3378...	-1002...	5.976...	5.347...	-2.621...	1.355...	59.79...	60.08...
16	FN	1-Phase-C	B2	Area 0	2958...	19260...	2326...	20293...	24.23...	20431...	-1763...	325.4...	-1685...	445.2...	-2730...	-781.5...	-3.662...	5.877...	-4.532...	-7.335...	59.66...	60.18...
17	FN	1-phase-B	G2	Area-1	11726...	14148...	11403...	14153...	11713...	14152...	-1730...	882.8...	-2268...	810.9...	-2280...	-325.7...	-2.759...	6.418...	-3.910...	1.784...	59.73...	60.11...
18	FN	1-phase-A	G2	Area-1	11387...	14169...	11829...	14172...	11792...	14171...	-1716...	2020...	-2505...	936.2...	-2162...	-704.1...	-4153...	6.254...	-3.884...	1.684...	59.72...	60.12...
19	FN	1-phase-B	G1	Area-1	12023...	13874...	12034...	13874...	12003...	13872...	-1606...	678.4...	-2065...	541.5...	-2562...	429.2...	1.261...	5.921...	-3.003...	1.586...	59.78...	60.11...
20	FN	1-phase-A	G1	Area-1	11970...	13893...	11985...	13896...	11952...	13894...	-1719...	1323...	-2239...	628.7...	-2530...	297.4...	-1.290...	5.885...	-2.979...	1.703...	59.77...	60.10...
21	FN	1-phase-C	G2	Area-1	11798...	14164...	11826...	14167...	11400...	14166...	-1714...	1542...	-2156...	874.6...	-4390...	-720.4...	-8179...	6.281...	-3.874...	1.697...	59.73...	60.12...
22	FN	1-phase-C	G1	Area-1	11994...	13891...	12008...	13894...	11975...	13892...	-1696...	1130...	-2011...	613.9...	-189.3...	1564...	-8943...	5.868...	-2.965...	1.683...	59.77...	60.09...
23	FU	3-phase	G2	Area-1	2549...	18049...	4686...	20506...	3317...	18994...	-1886...	2925...	-2977...	1779...	-3753...	2094...	-6.256...	7.758...	-5.703...	1.178...	59.26...	60.35...
24	FU	3-phase	G1	Area-1	2655...	17750...	3747...	20965...	4191...	18490...	-639.5...	2121...	-2944...	1655...	-1907...	2078...	-6.446...	7.685...	-4.550...	1.917...	59.27...	60.29...

Table 7.7. Decision tree Training Data for Voltage Classification Problem

No.	Class V Nominal	Fault Type (3p/1p) Nominal	Location Nominal	Area Nominal	Vamin Numeric	Vamax Numeric	Vbmin Numeric	Vbmax Numeric	Vcmin Numeric	Vcmax Numeric	Iamin Numeric	Iamax Numeric	Ibmin Numeric	Ibmax Numeric	Icmin Numeric	Icmax Numeric	Pmin Numeric	Pmax Numeric	Qmin Numeric	Qmax Numeric	Fmin Numeric	Fmax Numeric
1	NM	3-Phase	G3	Area-2	63449.60...	155261...	63804...	15446...	63718...	15489...	-3658...	383.3...	-1882...	1281...	418.4...	3351...	1.332...	6.625...	-8.709...	1.967...	59.35...	60.45...
2	NM	3-Phase	G4	Area-2	10197.64...	157047...	10256...	15668...	10208...	15718...	-2865...	574.2...	-1871...	2535...	-1621...	2657...	1.691...	6.196...	-5.341...	2.133...	59.28...	60.43...
3	NM	1-Phase-A	G3	Area-2	80873.58...	150789...	12199...	15055...	12176...	15052...	-1396...	343.5...	-1970...	-120.3...	730.8...	3144...	2.673...	6.404...	-6.163...	1.005...	59.63...	60.22...
4	NM	1-Phase-A	G4	Area-2	121051.0...	153904...	12149...	15364...	24848...	15367...	-2666...	321.3...	-1648...	685.6...	728.5...	3009...	2.198...	6.293...	-6.321...	1.725...	59.52...	60.30...
5	NM	1-Phase-B	G3	Area-2	121192.7...	150739...	81100...	15050...	12120...	15049...	-1317...	345.8...	-2045...	-215.9...	680.6...	3181...	2.625...	6.434...	-6.363...	1.030...	59.62...	60.23...
6	NM	1-Phase-B	G4	Area-2	120489.6...	154498...	24961...	15421...	12081...	15426...	-2778...	336.8...	-1682...	695.8...	634.4...	3082...	2.196...	6.333...	-6.667...	1.725...	59.51...	60.30...
7	NM	1-Phase-C	G3	Area-2	121785.885	150358...	12200...	15012...	81059...	15011...	-1290...	332.9...	-2000...	-192.2...	707.8...	3105...	2.647...	6.399...	-6.083...	1.024...	59.64...	60.23...
8	NM	1-Phase-C	G4	Area-2	24869.7909	153444...	12193...	15318...	12184...	15320...	-2607...	300.9...	-1618...	720.8...	735.9...	2933...	2.242...	6.264...	-6.062...	1.710...	59.54...	60.29...
9	VU2	3-Phase	B1	Area 0	2487.245...	174670...	6404...	20479...	4073...	18578...	-1955...	2663...	-2887...	1264...	-3322...	1814...	-6.022...	7.712...	-5.714...	1.188...	59.37...	60.3748
10	VU2	3-Phase	B2	Area 0	4.504817	184141...	6.964...	22343...	11.46...	20794...	-2655...	2613...	-1776...	6144...	-2742...	2356...	-9.114...	6.178...	-4.849...	9.407...	59.27...	60.75...
11	VU2	1-Phase-A	B1	Area 0	25647.08...	184962...	1169...	15555...	63102...	18891...	-1713...	1452...	-1934...	636.6...	-2408...	-1014...	6.356...	5.326...	-2.618...	1.334...	59.79...	60.08...
12	VU2	1-Phase-A	B2	Area 0	16.04132	192052...	2781...	17618...	88812...	21963...	-1714...	6618...	-1584...	431.2...	-2716...	-814.6...	-3.640...	5.820...	-4.567...	-7.184...	59.66...	60.17...
13	VU2	1-Phase-B	B1	Area 0	24731.421	181852...	1590...	15628...	50423...	18901...	-1748...	328.7...	-1812...	752.6...	-2340...	-917.4...	4.720...	5.397...	-2.629...	1.431...	59.78...	60.07...
14	VU2	1-Phase-B	B2	Area 0	4333.082...	193031...	8.336...	18105...	83542...	20465...	-1807...	330.0...	-1614...	3222...	-2742...	-663.2...	-3.662...	5.929...	-4.547...	-7.328...	59.65...	60.17...
15	VU2	1-Phase-C	B1	Area 0	21251.9909	184751...	1666...	15580...	62555...	18884...	-1717...	813.2...	-1741...	644.6...	-3378...	-1002...	5.976...	5.347...	-2.621...	1.355...	59.79...	60.08...
16	VU2	1-Phase-C	B2	Area 0	2958.415...	192603...	2326...	20293...	24.23...	20431...	-1763...	325.4...	-1685...	445.2...	-2730...	-781.5...	-3.662...	5.877...	-4.532...	-7.335...	59.66...	60.18...
17	NM	1-phase-B	G2	Area-1	117267.8...	141486...	11403...	14153...	11713...	14152...	-1730...	882.8...	-2268...	810.9...	-2280...	-325.7...	-2.759...	6.418...	-3.910...	1.784...	59.73...	60.11...
18	NM	1-phase-A	G2	Area-1	113871.7...	141697...	11829...	14172...	11792...	14171...	-1716...	2020...	-2505...	936.2...	-2162...	-704.1...	-4153...	6.254...	-3.884...	1.684...	59.72...	60.12...
19	NM	1-phase-B	G1	Area-1	120230.1...	138746...	12034...	13874...	12003...	13872...	-1606...	678.4...	-2065...	541.5...	-2562...	429.2...	1.261...	5.921...	-3.003...	1.586...	59.78...	60.11...
20	NM	1-phase-A	G1	Area-1	119704.9...	138931...	11985...	13896...	11952...	13894...	-1719...	1323...	-2239...	628.7...	-2530...	297.4...	-1.290...	5.885...	-2.979...	1.703...	59.77...	60.10...
21	NM	1-phase-C	G2	Area-1	117980.3...	141645...	11826...	14167...	11400...	14166...	-1714...	1542...	-2156...	874.6...	-4390...	-720.4...	-8179...	6.281...	-3.874...	1.697...	59.73...	60.12...
22	NM	1-phase-C	G1	Area-1	119942.5...	138914...	12008...	13894...	11975...	13892...	-1696...	1130...	-2011...	613.9...	-189.3...	1564...	-8943...	5.868...	-2.965...	1.683...	59.77...	60.09...
23	VU2	3-phase	G2	Area-1	2549.561...	180497...	4686...	20506...	3317...	18994...	-1886...	2925...	-2977...	1779...	-3753...	2094...	-6.256...	7.758...	-5.703...	1.178...	59.26...	60.35...
24	VU2	3-phase	G1	Area-1	2655.221...	177500...	3747...	20965...	4191...	18490...	-639.5...	2121...	-2944...	1655...	-1907...	2078...	-6.446...	7.685...	-4.550...	1.917...	59.27...	60.29...

46

Table 7.8. Ranking of Predictor Variables and Corresponding Accuracy in Frequency Classification Problem

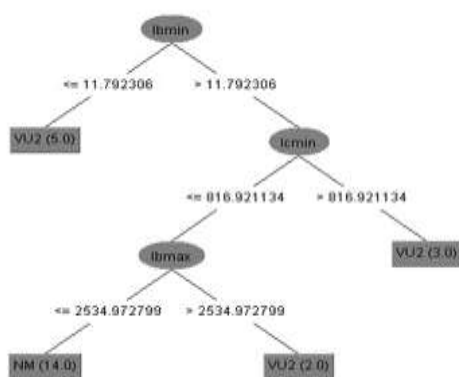| Rank	Predictor	Accuracy [Training Data used for Testing]	Accuracy [Cross Validation, 10 Folds]	Accuracy [Training 66%, Testing 34%]	Accuracy [Training 85%, Testing 15%]
1	Fmin	100	91.9167	100	100
2	Fmax, Ibmax, Area	97.9167	85.4167	75	85.7143
3	Icmax, Vamin, Fault Type	97.9167	87.5	75	100
4	Qmin, Area, Ibmax	97.9167	85.4167	75	85.7143
5	Vamax, Pmin, Pmax	97.9167	81.25	75	85.7143
6	Vbmax, Pmin, Pmax	97.9167	81.25	75	100
7	Vcmax, Pmin, Pmax	97.9167	83.33	75	100
8	Pmin, Fault Type, Vamin	100	85.4167	75	57.1429
9	Icmin, VO2b, Qmax, Fault Type	100	83.333	75	57.1429
10	Qmax, Area, Iamax	95.833	89.5833	75	57.1429
11	Location, VO2c, Fault Type	95.833	89.5833	75	57.1429
12	Area, Vamin, Iamax	95.833	85.4167	75	57.1429
13	Fault Type	87.5	81.25	75	57.1429
14	VO2b, Vamin, Pmax, VU2a, Vbmin, Iamin	100	70.833	62.5	71.4286
15	Vamin, Pmax, VU2a, Vbmin, Iamin	100	79.1667	56.25	85.7143
16	Vbmin, Pmax, VU2a, Vcmin, Vbmin, Iamin	100	77.0833	56.25	85.7143
17	Vcmin, Pmax	91.667	77.0833	62.5	85.7143
18	Ibmax, Iamin, VU2a	95.833	85.4167	56.25	100
19	Iamax, VU2a, Iamin	97.9167	83.333	56.25	100
20	Iamin, VO2c	89.5833	64.5834	56.25	71.4286
21	Ibmin, VU2c, Pmax, VU2a	95.8333	70.8333	56.25	71.4286
22	Pmax, VO2a	79.1667	56.25	56.25	71.4286

Table 7.9. Ranking of Predictor Variables and Corresponding Accuracy in Voltage Classification Problem

Rank	Predictor	Accuracy [Training Data used for Testing]	Accuracy [Cross Validation, 10 Folds]	Accuracy [Training 66%, Testing 34%]	Accuracy [Training 85%, Testing 15%]
1	VU2a	100	100	100	100
2	Vamax	100	91.6667	87.5	85.7143
4	Vcmax	100	91.6667	87.5	85.7143
5	VU2b, VO2b	100	91.6667	87.5	85.7143
6	VO2c, VO2b	100	95.833	100	100
7	Vbmin, Vbmax	100	95.833	100	100
8	VO2a, VU2c	100	97.9167	100	100
9	VU2c, Icmax, Area	100	87.5	75	100
10	VO2b, Icmax, Area	100	93.75	93.75	100
11	Vbmax, Icmin	100	93.75	93.75	100
12	Icmin, Vamin	100	95.833	87.5	100
13	Vamin, Area	100	93.75	87.5	100
14	Area, Vcmin	100	89.5833	93.75	100
15	Icmax, Ibmin, Location, Iamin	100	81.25	93.75	85.7143
16	Vcmin, Location, Iamin	100	89.5833	87.5	85.7143
17	Iamin, Pmin, Pmax	100	93.75	87.5	100
18	Ibmin, Pmin, Pmax	100	91.667	87.5	100
19	Location, Ibmax, Iamax, Qmax	93.75	77.0833	75	85.7143
20	Pmax, Pmin, Fault Type	100	66.6667	75	71.4286
21	Fault type, Iamax, Pmin, Ibmax	100	66.6667	75	71.4286
22	Pmin, Qmin, Ibmax	100	85.4167	75	85.7143
23	Qmin, Ibmax, Iamax	100	72.9167	68.75	85.7143
24	Qmax, Iamax	97.9167	79.1667	68.75	85.7143

Fig.7.3-Fig.7.10 presents some of the sample decision tree structures obtained from the analysis so far along with their associated predictor variables and the corresponding accuracies from the four methods mentioned above.

Fig.7.3 represents the application of current measurements in detecting the violations in voltage standards mentioned in IEEE 1547. Fig.7.4 represents a combination of real and reactive power measurements along with current measurements to predict the voltage standard violations. The figures also include the accuracy values from the four different methods used to test the developed decision trees along with the predictors used. The maximum accuracy among the different testing methods (cross validation, percent split- 66, 34 and percent split-85, 15) is 100% and the minimum is 70.83%. The accuracy values indicates that these combinations can be utilized to predict the voltage violation events even though the voltage measurements are not available for the classification and prediction purpose.Fig.7.5 and Fig.7.6 presents the utilization of combinations of voltage and current measurements, and voltage and power measurements in detecting the abnormal frequency events. The maximum accuracy among the different testing methods (cross validation, percent split- 66, 34 and percent split-85, 15) is 83.33% and the minimum is 67.55%. The accuracy values presents the possibilities of utilizing the voltage and power measurements in detecting frequency abnormalities with reasonable accuracies.Fig.7.7 and Fig.7.8 presents the use of combination of voltages, currents and power measurements along with fault types to predict the frequency abnormalities for microgrid islanding purpose. These cases include training data consisting of 24 different contingencies under two different loading conditions in the microgrid. The maximum and minimum accuracies are 100% and 75%, respectively from the three different testing approaches employed.
Fig.7.9 and Fig.7.10 shows the use of current and power measurements in classification of voltage abnormalities. These cases also include training data consisting of 24 different contingencies under two different loading conditions in the microgrid. The maximum and minimum accuracies are 100% and 66.67%, respectively from the three different testing approaches employed.

These experiments indicates the abilities of decision trees in classification and prediction of relevant events even when the most relevant or important measurements are not available. There might be a compromise in the classification and prediction accuracies, but the accuracies in the experiments indicates that the decision trees still achieve reasonable accuracies and these values can be further improved with the enhancements (i.e. including more contingency cases) of the training dataset.

Predictors	Ibmin, Icmin, Ibmax
Accuracy(training data)	100 %
Accuracy(Cross Validation)	70.833%
Accuracy (% Split-66,34)	100%
Accuracy (% Split-85,15)	100%

(a)
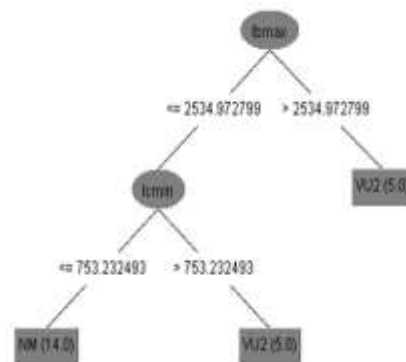
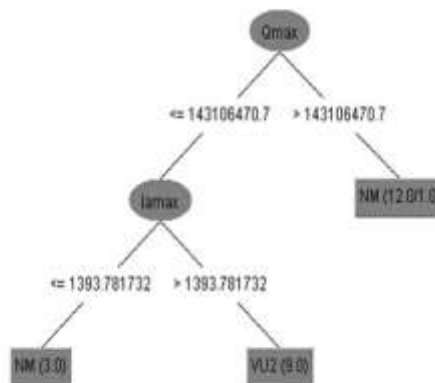| Predictors	Ibmax, Icmin
Accuracy(training data)	100 %
Accuracy(Cross Validation)	87.5%
Accuracy (% Split-66,34)	100%
Accuracy (% Split-85,15)	100%

(b)

Figure 7.3. Decision trees for voltage classification: (a) with predictors Ibmin, Icmin, Ibmax; (b) with predictors Ibmax and Icmin

Predictors	Icmin, Pmax, Qmax
Accuracy(training data)	95.83 %
Accuracy(Cross Validation)	79.17%
Accuracy (% Split-66,34)	100%
Accuracy (% Split-85,15)	100%

(a)

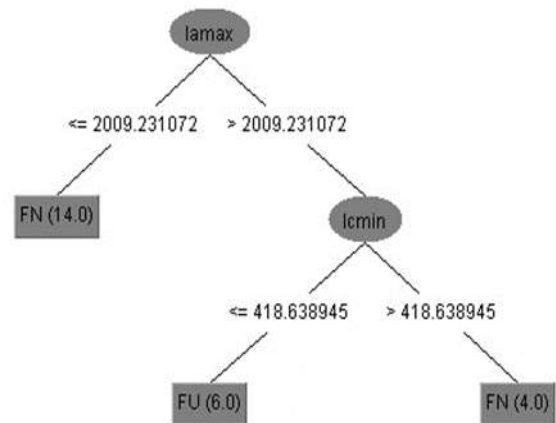| Predictors	Qmax, Iamax
Accuracy(training data)	95.83%
Accuracy(Cross Validation)	83.33%
Accuracy (% Split-66,34)	100%
Accuracy (% Split-85,15)	100%

(b)

Figure 7.4. Decision trees for voltage classification: (a) with predictors Icmin, Pmax and Qmax; (b) with predictors Qmax and Iamax
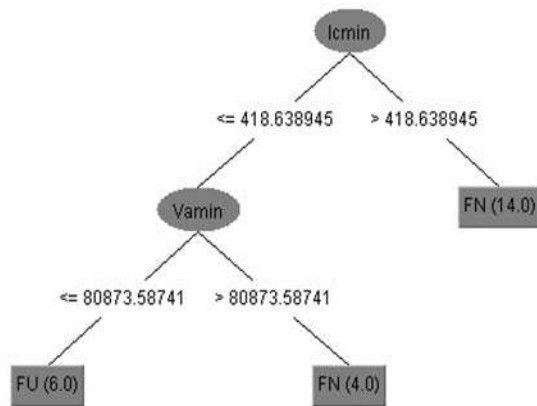
Predictors	Icmin, Vamin
Accuracy(training data)	100 %
Accuracy(Cross Validation)	83.33%
Accuracy (% Split-66,34)	75%
Accuracy (% Split-85,15)	75%

(a)

Predictors	Iamax, Icmin
Accuracy(training data)	95.83 %
Accuracy(Cross Validation)	79.17%
Accuracy (% Split-66,34)	75%
Accuracy (% Split-85,15)	72%

(b)

Figure 7.5. Decision trees for frequency classification: (a) with predictors Icmin and Vamin; (b) with predictors Iamax and Icmin
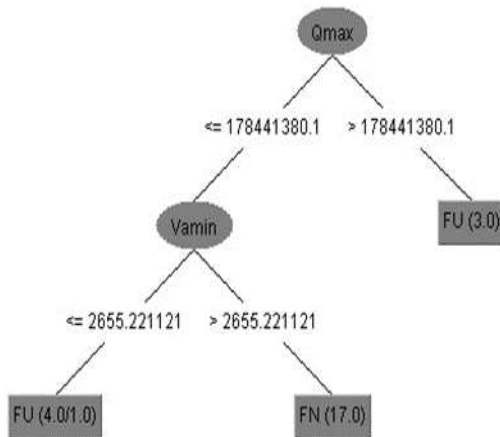
Predictors	Qmax, Vamin
Accuracy(training data)	95.83 %
Accuracy(Cross Validation)	79.17%
Accuracy (% Split-66,34)	75%
Accuracy (% Split-85,15)	67.55%

(a)

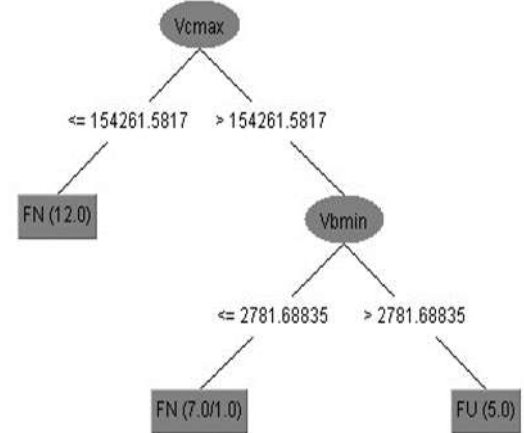| Predictors	Vcmax, Vbmin
Accuracy(training data)	95.83 %
Accuracy(Cross Validation)	70.833%
Accuracy (% Split-66,34)	75%
Accuracy (% Split-85,15)	67.55%

(b)

Figure 7.6. Decision trees for frequency classification: (a) with predictors Qmax and Vamin; (b) with predictors Vcmax and Vbmin

51
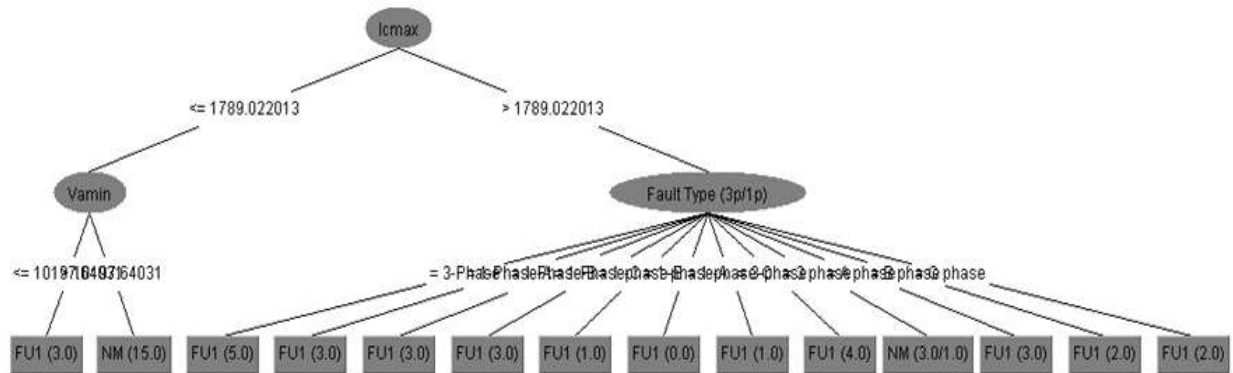
Predictors	Icmax, Vamin, Fault Type
Accuracy(training data)	97.92 %
Accuracy(Cross Validation)	87.50%
Accuracy (% Split-66,34)	75%
Accuracy (% Split-85,15)	100%

Figure 7.7. Decision trees for frequency classification with predictors Icmax, Vamin and Fault types
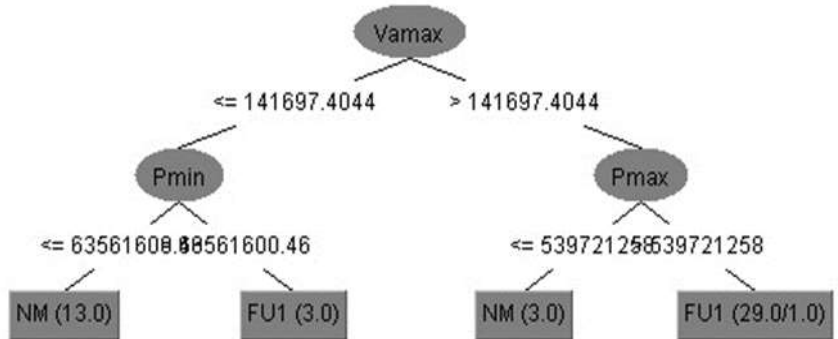
Predictors	Vamax, Pmin, Pmax
Accuracy(training data)	97.92 %
Accuracy(Cross Validation)	81.25%
Accuracy (% Split-66,34)	75%
Accuracy (% Split-85,15)	85.72%

Figure 7.8. Decision trees for frequency classification with predictors Vamax, Pmin and Pmax

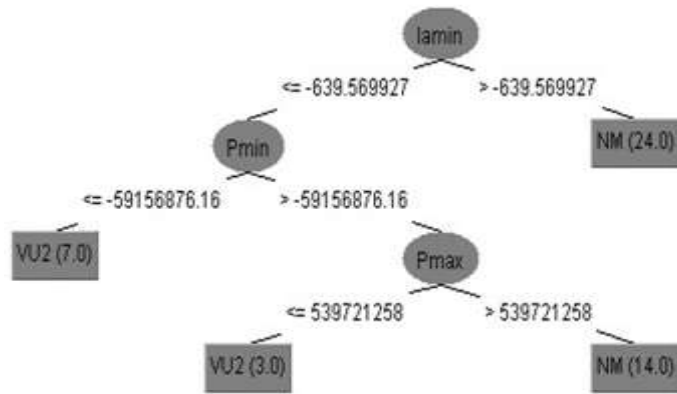| Predictors	Iamin, Pmin, Pmax
Accuracy(training data)	100 %
Accuracy(Cross Validation)	93.75%
Accuracy (% Split-66,34)	87.5%
Accuracy (% Split-85,15)	100%

Figure 7.9. Decision trees for voltage classification with predictors Iamin, Pmin and Pmax
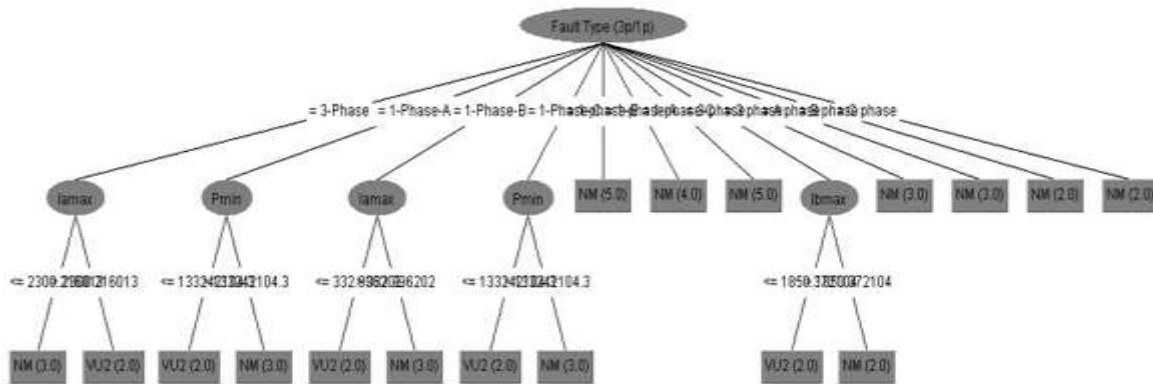
Predictors	Fault Type, Iamax, Pmin, Ibmax
Accuracy(training data)	100 %
Accuracy(Cross Validation)	66.67%
Accuracy (% Split-66,34)	75%
Accuracy (% Split-85,15)	71.43%

Figure 7.10. Decision trees for voltage classification with predictors Fault types, Iamax, Pmin and Ibmax

CHAPTER 8
CONCLUSION AND RECOMMENDATIONS

The microgrid will play a very vital role in the future grid-system and the penetration of distributed generators will increase more than ever. Therefore, it is very important to study the impact of this distributed generation penetration for ensuring a more reliable and efficient power grid system. In this thesis work, three distributed generators were connected to form a microgrid capable of stable operation in both grid-connected and islanding mode. All three DGs model developed in Simulink MATLAB satisfy the current harmonics and DC injection standards set by IEEE 1547 Standard for interconnection with the main grid system. Battery control was designed for load shaving during peak hours of load when the load increases from the planned load. The control strategies in these DGs is developed in such a way that the microgrid is capable of functioning properly in grid-mode and also, capable of independently working in islanding-mode. In grid-connected mode, all DGs follow the frequency of the main grid whereas in islanding-mode, the diesel generator provides the reference frequency which the other DGs follow. Various scenarios of possible contingencies in this microgrid system in both grid-connected and islanding mode were studied. The microgrid was connected to Kundur's two area system to better emulate the behavior of the main power system. The results were analyzed to better understand the behavior of DGs in the microgrid as well as the generators in the Kundur's two-area system. Four cases of such contingency simulations are discussed in this thesis work. The study of these contingencies gives a better understanding of the behavior of distributed generators.

To further this study, another distributed generator e.g. wind turbine can be added to this system to further study the behavior of microgrid and main grid under different scenarios. Also, since the load in IEEE 13 Node Test Feeder System is unbalanced therefore negative sequence compensators can be implemented in the power electronics converter of any DG to improve the voltage and current waveforms in the microgrid.

For the purpose of developing a decision trees based protection and control framework or fault-detection algorithm for microgrids against disturbances, various cases of contingencies in external grid were simulated with the microgrid in grid-connected mode. The data was collect at PCC and from this data, a list of critical attributes was developed which includes the parameter likely to be of concern in terms of security etc. Weka software is a collection of machine learning algorithms for data mining tasks. Weka contains tools for data pre-processing, classification, regression, clustering, association rules, and visualization. It is also well-suited for developing new machine learning schemes. Decision trees are trained to detect underlying patterns and relationships among various system parameter which can be used for predicting system voltages and frequency following contingencies for assisting the islanding decision process. The decision trees using this software point out to the parameters which are likely to predict the violation of any security criteria for islanding. Fault information and voltage/frequency measurements at the PCC bus have the highest rankings. If fault information or voltage/frequency measurements are not available, current, real power or reactive power measurements can be alternatives to help make the decision.

The 48 cases simulations and decision tree development done in this thesis work show the potential of decision trees in classification and prediction of concerned events even when the most relevant or important measurements are not available. There may be some compromises in the classification and prediction accuracies, but the results show that they are still reasonable and can be made more reliable by adding more possible cases. A bigger database can thus further be developed to build, refine and improve the decision trees. This larger database can be used to include all the possible contingencies and scenarios to make these decision trees more and more reliable and practical.

LIST OF REFERENCES

[1] The World Alliance for Decentralized Energy (WADE), *World Survey on Decentralized Energy 2006*, 46 pages, May 2006 (source: http://www.localpower.org)

[2] R. H. Lasseter, et al., "White paper on integration of distributed energy resources, The CERTS microgrid concept." *Consortium for Electric Reliability Technology Solutions*, pp. 1-27, 2002.

[3] L. Blackburn, T. J. Domin, "Protective relaying – Principles and Applications," Third Edition, CRC Press, 2006.

[4] M. R. Islam, H. A. Gabbar, "Analysis of Microgrid Protection Strategies," *IEEE International Conference on Smart Grid Engineering*, August, 2012.

[5] C. Marnay, F. Rubio, and A. Siddiqui, "Shape of the microgrid", *IEEE Power Engineering Society Winter Meeting*, Vol. 1, pp.150 - 153, 2001.

[6] "IEEE 13 Node Test Feeder System,"(source: http://ewh.ieee.org/soc/pes/dsacom/testfeeders/)

[7] "Commercial Opportunities for Back-Up Generation and Load Reduction via National Grid, the National Electricity Transmission System Operator (NETSO) for England, Scotland, Wales and Offshore," 2009-12-22. Retrieved 2012-07-13(source: www.claverton-energy.com).

[8] U. Gangopadhyay, S. Jana, and S. Das, "State of Art of Photovoltaic Technology*," Conference Papers in Energy*, Volume 2013 (2013), Article ID 764132, 9 pages, (source: http://dx.doi.org/10.1155/2013/764132).

[9] R.N.Tripathi, A. Singh, M.Badoni, " A MATLAB Simulink based Solar Photovoltaic Array SPVA module with MPPT,"*Emerging Trends in Communication, Control, Signal Processing & Computing Applications (C2SPCA)*, 2013 International Conference onOct. 2013.

[10] O. Tremblay, L. Dessaint,"Experimental Validation of a Battery Dynamic Model for EV Applications," *EVS24 Stavanger, Norway*, May 13 - 16, 2009

[11] Y.Iijima, Y. Sakanaka, N. Kawakami, M. Fukhuhara, "Development and field experiences of NAS battery inverter for power stabilization of a 51 MW wind farm", *Power Electronics Conference (IPEC)*, 2010 International, Page(s): 1837-1841.

[12] Y.Liu, "Improvement of Available Battery Capacity,"*Journal of Power Electronics*, Vol. 13, No. 3, May 2013.

[13] H. Bai, C. Mai, "The impact of bidirectional DC-DC converter on the inverter operation and battery current in hybrid electric vehicles",*Power Electronics and ECCE Asia (ICPE & ECCE), 2011 IEEE 8th International Conference* onMay 2011-June2011, Page(s): 1013-1015.

[14] M.A Sofla, L. Wang,"Control of DC-DC Bidirectional Converters for Interfacing Batteries in Microgrid,"*Power Systems Conference and Exposition (PSCE), 2011 IEEE/PES* on March 2011, Page(s): 1-6.

[15] *IEEE Application Guide for IEEE Std. 1547™- IEEE Standard for Interconnecting Distributed Resources with Electric Power Systems*, IEEE Std. 1547-2003, Jun. 2003.

[16] Y.Wang, Z. Lu, Y. Min, "Analysis and comparison on the control strategies of multiple voltage source converters in autonomous microgrid", Developments in Power System Protection (DPSP 2010). Managing the Change, 10th IET International Conference, 2010 , Page(s): 1- 5.

[17]   C. Liu, Z.H. Rather, Z. Chen, C. L. Bak, "An Overview of Decision Tree Applied to Power System", *Intl. Journal of Smart Grid and Clean Energy, vol.2, no.3, pp.414-419, Oct. 2013.*

[18]   L. Wenhenkel, M. Pavella, "Advances in Decision Trees Applied to Power System Security Assessment", *in Proc. IEE Advances in Power System Control, Operation and Management, Dec. 1993, pp.47-53*

[19]   K. Sun, S. Likhate, V. Vittal, V.S. Kolluri, S. Mandal, "An Online Dynamic Security Assessment Scheme Using Phasor Measurements and Decision Trees*", IEEE Trans. on Power Systems, vol.22, no.4, pp.1935-1943, Nov. 2007.*

[20]   K. E. Arroudi, G. Joos, "Data Mining Approach to Threshold Setting of Islanding Relays in Distributed Generation", *IEEE Trans. on Power Systems, vol.22, no.3, pp.1112-1119, Aug. 2007.*

[21]   P.Kundur Author, "Power System Stability and Control," 1994.

[22]   C. Tammineedi, " Modeling battery-ultracapacitor hybrid system for solar and wind application," 2011 Thesis , Available: https://etda.libraries.psu.edu/paper/11561/6886

VITA

Hira Amna Saleem received her B.Sc. degree in Electronics engineering from Ghulam Ishaq Khan Institute of Science and Technology, Pakistan, in 2010. This thesis is the work done for the partial fulfillment of her M.Sc degree in Electrical Engineering at the University of Tennessee, Knoxville.